論文 / 著書情報
Article / Book Information

題目(和文)	BiFeO3系薄膜の圧電およびマルチフェロイック特性
Title(English)	Piezoelectric and multiferroic properties of BiFeO3-based thin films
著者(和文)	清水啓佑
Author(English)	Keisuke Shimizu
出典(和文)	学位:博士(理学), 学位授与機関:東京工業大学, 報告番号:甲第10745号, 授与年月日:2018年3月26日, 学位の種別:課程博士, 審査員:東 正樹,舟窪 浩,吉本 護,谷山 智康,笹川 崇男
Citation(English)	Degree:Doctor (Science), Conferring organization: Tokyo Institute of Technology, Report number:甲第10745号, Conferred date:2018/3/26, Degree Type:Course doctor, Examiner:,,,,
学位種別(和文)	博士論文
Type(English)	Doctoral Thesis

Piezoelectric and multiferroic properties of $BiFeO_3$-based thin films

($BiFeO_3$ 系薄膜の圧電およびマルチフェロイック特性)

Keisuke Shimizu

A thesis

Department of Innovative and Engineered Materials

Interdisciplinary Graduate School of Science and Engineering

Tokyo Institute of Technology

Supervisor: Professor Masaki Azuma

February, 2018

Table of Contents

Chapter 1 General introduction

1.1 Preface

Bi-containing perovskite oxides, BiBO$_3$, have received much attention as candidates for lead-free piezoelectric/ferroelectric and multiferroic materials. In these materials, ferroelectricity is induced by a stereochemically active Bi^{3+} ion with $6s^2$ lone pair in A site of perovskite ABO_3. Therefore, in contrast to typical piezoelectric/ferroelectric materials where d^0-ness in B site is required to induce ferroelectricity, there is a high degree of freedom for B site cation-selectivity in these materials. Many Bi-containing perovskite oxides have been synthesized, such as $BiFeO_3$, $BiAlO_3$, $BiMnO_3$, $BiCoO_3$, $BiZn_{1/2}Ti_{1/2}O_3$, and so on [1-5]. Among them, antiferromagnetic ferroelectric material $BiFeO_3$ has been studied most extensively as lead-free piezoelectric material or multiferroic material [1,6-8].

This material is regarded as a promising candidate for the replacement of the most widely used piezoelectric material Pb(Zr,Ti)O$_3$ (PZT). The problem is the low piezoelectric response [6]. The polarization rotation observed in monoclinic PZT is considered to be a key factor to improve the piezoelectric response of lead-free piezoelectric material. In this thesis, Co and Ga substituted $BiFeO_3$ are selected as research targets and the relationship between the piezoelectric response and the polarization rotation is investigated in detail. Moreover, the orientation dependence is examined in Ga-substituted $BiFeO_3$.

As multiferroic material, $BiFeO_3$ is expected to be applied in low energy consumption memory devices where a magnetization is controlled by application of electric field [9]. Although $BiFeO_3$ has an antiferromagnetic order with no net magnetization at room temperature, Co-substitution induces ferromagnetic spontaneous moment due to spin canting by Dzyaloshinskii-Moriya (DM) interaction [9,10]. Therefore, the moment is expected to be controlled by the electric polarization switching. Although the macroscopic reorientation behavior of the magnetic domains by polarization switching had been confirmed, the direct observation of local magnetization reversal was absent [11]. In this thesis, the detailed switching mechanism of a magnetization reversal by polarization switching in Co-substituted $BiFeO_3$ thin films is investigated.

1.2 Bi-based lead-free piezoelectric materials

Piezoelectric materials, which has no inversion symmetry and can convert mechanical energy into electric one, or vice versa, are used in sensors, actuators, and transducers. Among them, $PbZr_xTi_{1-x}O_3$ (PZT) is the most widely used piezoelectric material due to the high piezoelectric response and high operating temperature. This material, discovered by Shirane *et al.* in 1952, is a solid solution of ferroelectric $PbTiO_3$ and antiferroelectric $PbZrO_3$ [12]. Ferroelectric $PbTiO_3$ has a tetragonal structure with a pyramidally coordinated TiO_5 (space group *P*4*mm*), where the polarization points to the [001] direction. $PbZrO_3$ has an antiferroelectric orthorhombic structure (space group *Pbam*). Zr substitution for Ti in $PbTiO_3$ induces the structural transition in the following sequence [13] (Fig. 1-1); ferroelectric tetragonal phase ($0 \leq x \leq 0.52$) → ferroelectric rhombohedral phase ($0.52 \leq x \leq 0.94$) → antiferroelectric orthorhombic phase ($0.94 \leq x \leq 1$). The compositional phase boundary ($x \sim 0.48$) between tetragonal and ferroelectric rhombohedral phases is known as morphotropic phase boundary (MPB). Jaffe *et al.* discovered that the piezoelectric response was drastically enhanced at MPB [14] as shown in Fig.1-2. In 2000, Noheda *et al.* reported that the structure of PZT at MPB composition was a monoclinic one with space group *Cm* [15].

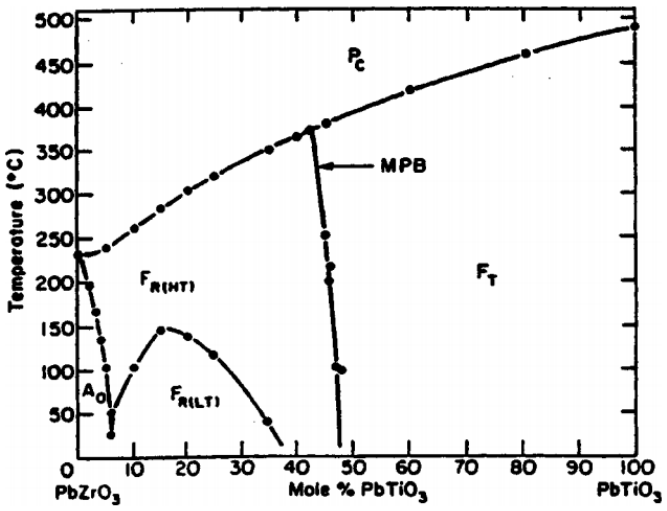

Figure 1-1 Crystal structure phase diagram for $Pb(Zr,Ti)O_3$ [13,15].

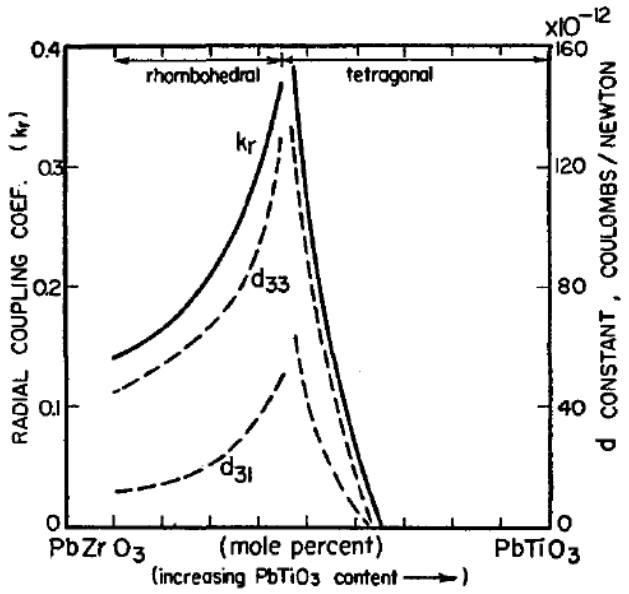

Figure 1-2 Piezoelectric constant for $Pb(Zr,Ti)O_3$ [14].

It is theoretically explained that the enhanced piezoelectric response at MPB is due to a polarization rotation induced by the application of electric field in the monoclinic phase [16]. In rhombohedral and tetragonal phases, the polarization directions are constrained along a polar axis, that is, [111] and [001], respectively [17-19]. Therefore the polarization does not rotate easily by application of electric field. On the other hand, , the polarization direction of a lower-symmetric monoclinic phase is not constrained and can rotate easily by application of electric field because a symmetry axis is vanished. Monoclinic phases are categorized into three, *i.e.* M_A, M_B, and M_C named by Vanderbilt and Cohen. The polarization direction points between [001] and [111], between [111] and [110], and between [001] and [101] in the M_A, the M_B, and the M_C phases, respectively. It is theoretically suggested that a larger piezoelectric response at a low electric bias is expected in the M_A phase, which is the same as the monoclinic PZT at the MPB.

Currently PZT is the most widely used piezoelectric material. However, because PZT contains the toxic element lead, there is a growing demand for the replacement of PZT with lead-free piezoelectric materials.

The origin of ferroelectricity in PZT is not only the second order Jahn-Teller active Ti^{4+} and Zr^{4+} with a d^0 configuration, but also a stereochemically active Pb^{2+} cation with $6s^2$ lone pair [20,21]. $6s^2$ lone pair in Pb^{2+} plays a crucial role in enhancement of the

ferroelectric strain because it is strongly hybridized with O 2*p* orbitals: Both $PbTiO_3$ and $BaTiO_3$ have a polar tetragonal structure at room-temperature, but the ferroelectric strain of $PbTiO_3$ (*c*/*a* ~1.067) is much larger than that of $BaTiO_3$ (*c*/*a* ~1.01) as shown in Fig1-3.

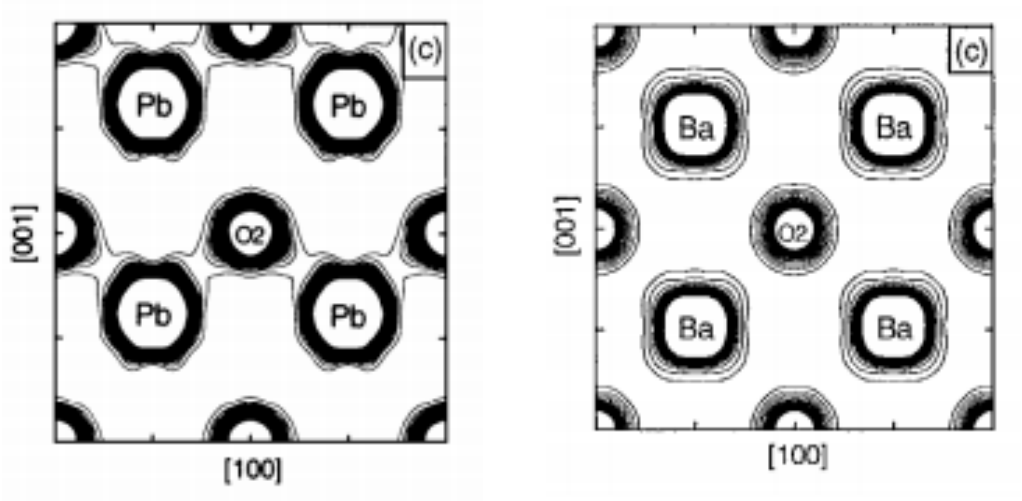

Figure 1-3 MEM charge-density distributions of $PbTiO_3$ (left) and $BaTiO_3$ (right). It is clearly seen that Pb cation is strongly hybridized with O 2*p* states [21].

Bi-containing perovskites has been considered to be candidate lead-free piezoelectric materials for the replacement of PZT, because Bi^{3+} cation has a same electronic configuration as Pb^{2+} and has a low toxicity. Many polar Bi-containing perovskite oxides have been synthesized, such as $BiFeO_3$, $BiAlO_3$, $BiCoO_3$, $BiInO_3$, $BiZn_{1/2}Ti_{1/2}O_3$, $BiZn_{1/2}V_{1/2}O_3$, and so on [1-3,5,22,23]. Among them, $BiFeO_3$ is the most extensively studied material because that is the only Bi-containing simple perovskite which can be synthesized at ambient pressure [24]. This material is a ferroelectric rhombohedral perovskite (Space group *R*3*c*) (shown in Fig. 1-4) with a high ferroelectric Curie temperature (~1100 K) and a large spontaneous polarization (~100 μC/cm^2) along the [111] direction. The lattice parameter a_{pc} and α are 3.965 Å and 89.4°, respectively [1]. The piezoelectric constant d_{33} is reported to be about 60 pm/V in thin film samples (shown in Fig. 1-5), which is much smaller than that of monoclinic PZT thin films [6,25,26]. Therefore, an improvement of the piezoelectric response is necessary for the practical use. There have been many attempts to improve the piezoelectric property of $BiFeO_3$ by element substitution [27-29]. It is suggested that a realization of a monoclinic phase with polarization rotation is a promising concept to improve the piezoelectric

response. In this thesis, Co and Ga substituted $BiFeO_3$ is selected as target compounds because both materials have a monoclinic phase same as that of monoclinic PZT.

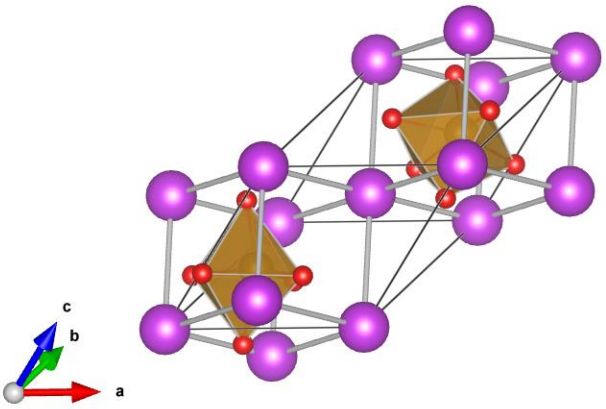

Figure 1-4 Crystal structure of $BiFeO_3$ illustrated with VESTA[30]. Purple, yellow, red spheres stand for Bi, Fe, and O ions, respectively.

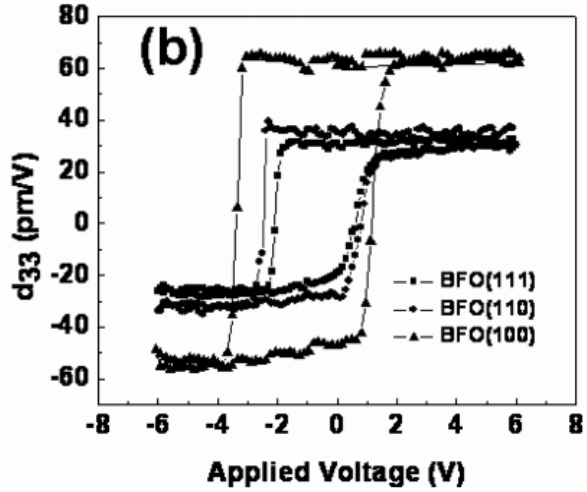

Figure 1-5 Piezoelectric constant d_{33} of $BiFeO_3$ thin films[26].

$BiCoO_3$ was synthesized using a high temperature high pressure method by A. Belik *et al* [5]. The material has a $PbTiO_3$-type tetragonal perovskite structure with a CoO_5 pyramidal coordination but the tetragonal strain (c/a ~1.26) is much larger than that of $PbTiO_3$ (~1.067) as illustrated in Fig. 1-6. This is due to a presence of a Co^{3+} cation with a high spin $3d^6$ configuration (shown in Fig. 1-7). Since one of the six apical oxygen anions is close to the Co cation in the pyramidal coordination, the energy of d_{xy} orbital is lowered than that of d_{yz} and d_{zx} orbitals [31,32]: Five electrons out of six occupy all of the five 3d orbitals according to Hund's rule, and the remaining one down spin electron occupy the d_{xy} orbital with a lowest energy level. Therefore a large energy is gained in this configuration. This material has a high curie temperature and a large spontaneous polarization due to the large strain.

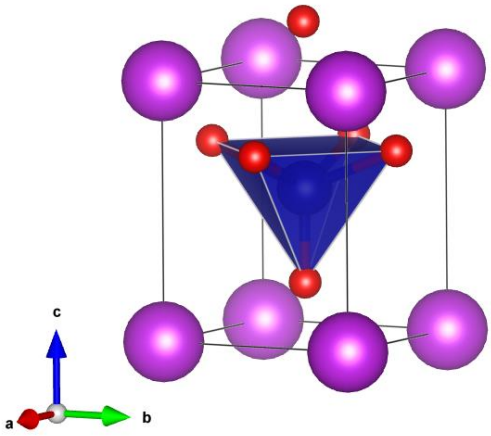

Figure 1-6 Crystal structure of $BiFeO_3$ illustrated with VESTA[30].
Purple, blue, red spheres denotes Bi, Co, and O ions, respectively.

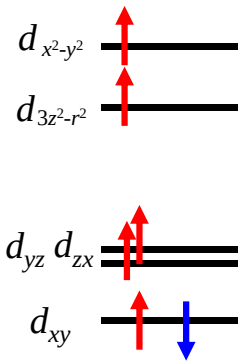

Figure 1-7 Electronic configuration in tetragonal $BiCoO_3$.

M. Azuma *et al*. successfully prepared a solid solution between $BiFeO_3$ and $BiCoO_3$ ($BiFe_{1-x}Co_xO_3$ or BFCO) [33]. They confirmed that this material had a MPB between rhombohedral and tetragonal phase ($x \sim 0.3$) and a monoclinic phase with $\sqrt{2}a \times \sqrt{2}a \times a$ unit cell where a is the lattice parameter of a cubic perovskite structure near the MPB as shown in Fig.1-8. The monoclinic phase has a large tetragonal(-like) strain and a large polarization comparable to that of $BiCoO_3$. Thereafter, K. Oka *et al*. has revealed that the monoclinic phase has the same *Cm* space group as that of monoclinic PZT and a polarization rotation between [001] and [111] occurs as functions of temperature and composition [34] as shown in Fig.1-9 and 1-10. An enhanced piezoelectric response is expected in the monoclinic $BiFe_{1-x}Co_xO_3$. Piezoelectric response of $BiFe_{1-x}Co_xO_3$ thin films have been reported in some papers [28,35-37]. However, the $BiFeO_3$-related rhombohedral phase is focused in most of the papers. Only Nakamura *et al*. succeeded in preparation of thin films with a giant c/a ratio using chemical solution deposition method and evaluating the piezoelectric properties. However, their film had low crystallinity and a monoclinic distortion was not observed. Therefore it is unclear whether the piezoelectric response of the monoclinic BFCO thin films is enhanced or not.

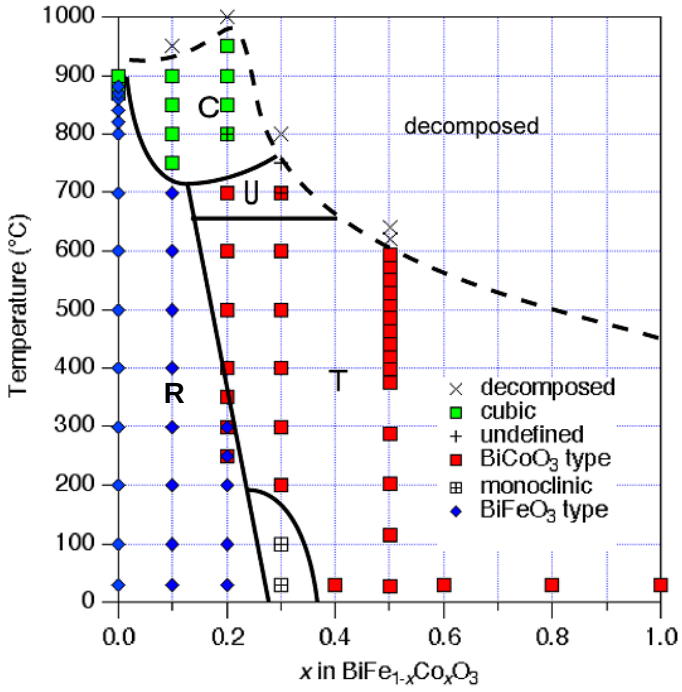

Figure 1-8 Crystal structure phase diagram for $BiFe_{1-x}Co_xO_3$ [33].

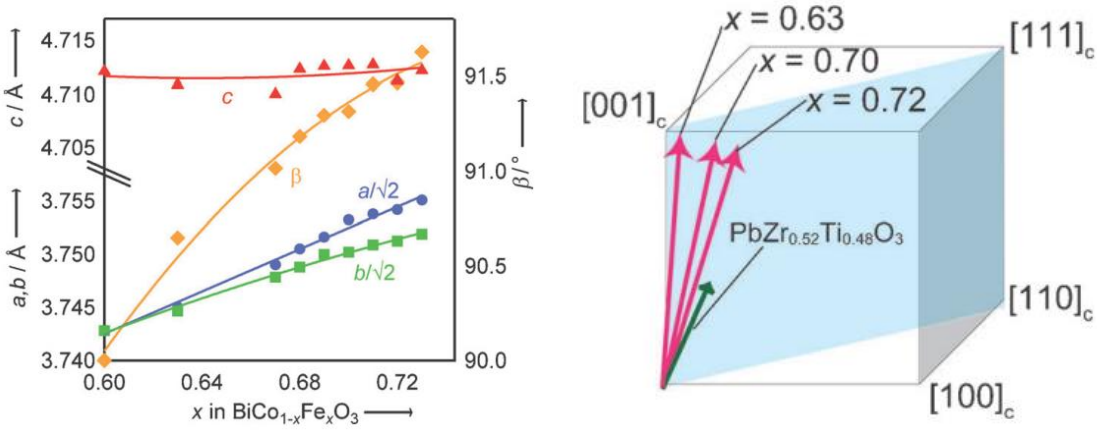

Figure 1-9 Composition dependence of the lattice parameters (left) and the polarization direction calculated by point charge model for $BiCo_{1-x}Fe_xO_3$ near MPB [31].

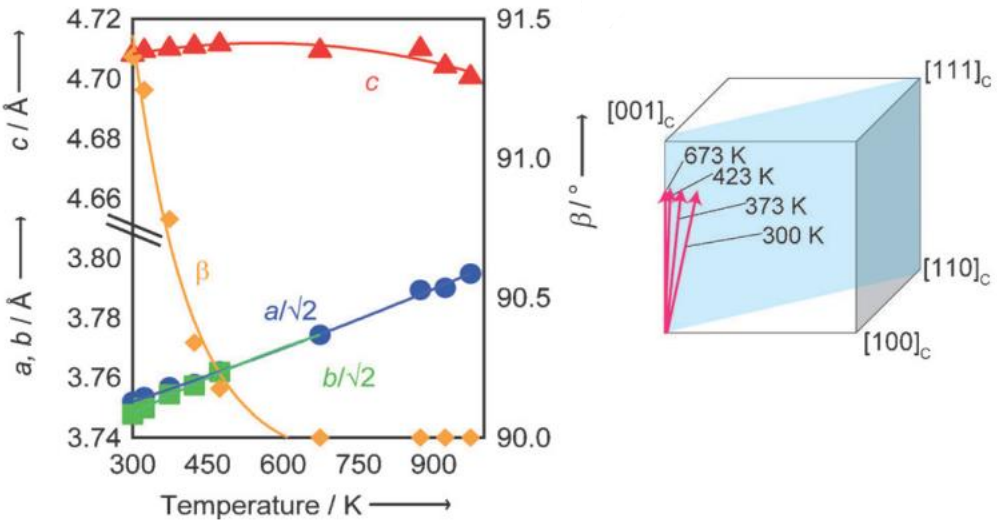

Figure 1-10 Temperature dependence of the lattice parameters (left) and the polarization direction calculated by point charge model for $BiCo_{1-x}Fe_xO_3$ near MPB [31]

$BiGaO_3$ was synthesized using a high temperature high pressure method by A. Belik *et al* [3]. $BiGaO_3$ has a non-perovskite structure with GaO_4 tetrahedral coordination, known as pyroxene as illustrated in the left panel of Fig. 1-11. It was found that the pyroxene phase was transformed into a perovskite phase under high pressure conditions above 3.2 GPa, although this phase was unquenchable to ambient pressure [38]. The perovskite phase preserved a polar monoclinic phase (space group; *Cm*) with a giant *c*/*a* ratio the same as that of Co-substituted $BiFeO_3$ below 6.3 GPa. A. Belik *et al*. successfully synthesized perovskite-type $BiGa_xM_{1-x}O_3$ (*M*=Cr, Mn, and Fe) which was stable even at ambient pressure[39]. The structural phase diagrams are shown in Fig. 1-12. All of these systems have the monoclinic phase with a giant *c*/*a* ratio the same as those of perovskite-type $BiGaO_3$ and the monoclinic $BiFe_{1-x}Co_xO_3$ as illustrated in the right panel of Fig. 1-11. An enhanced piezoelectric response is therefore expected in the monoclinic $BiFe_{1-x}Ga_xO_3$.

To evaluate the piezoelectric properties of the $BiFeO_3$-based materials, single crystalline epitaxial thin film samples are indispensable because of the high leakage current at grain boundary of the ceramic samples. Although the monoclinic phases with a giant *c*/*a* ratio can be prepared by high pressure synthesis method as bulk samples, it was reported that pure $BiFeO_3$ thin films on substrates with a small lattice constant (a_{pc} < 3.79 Å), such as $LaAlO_3$, crystalized in a monoclinic structure with a giant *c*/*a* ratio[40,41]. Since the *c*/*a* ratio is similar to that of the monoclinic $BiFe_{1-x}Co_xO_3$ and $BiFe_{1-x}Ga_xO_3$, it is expected that the monoclinic phases can be prepared on $LaAlO_3$ substrate. In this thesis, the monoclinic $BiFe_{1-x}Co_xO_3$ and $BiFe_{1-x}Ga_xO_3$ are prepared on $LaAlO_3$ substrate and their crystal structure and piezoelectric response are evaluated.

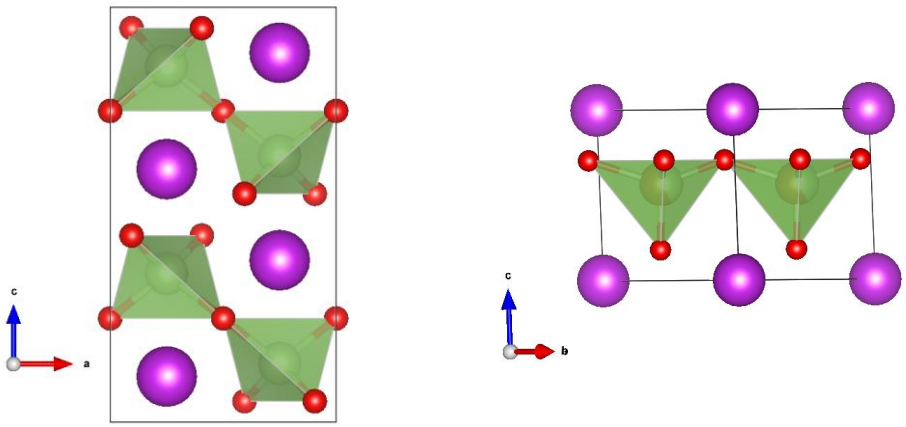

Figure 1-11 Crystal structure of pyroxene $BiGaO_3$ (left) and monoclinic perovskite $BiFe_{0.6}Ga_{0.4}O_3$ (right) illustrated with VESTA[30]. The polarization in monoclinic phase tilts from $[001]_{pc}$ toward $[\bar{1}\bar{1}0]_{pc}$ direction. Purple, green, yellow, red spheres denotes Bi, Ga, Fe, and O ions, respectively.

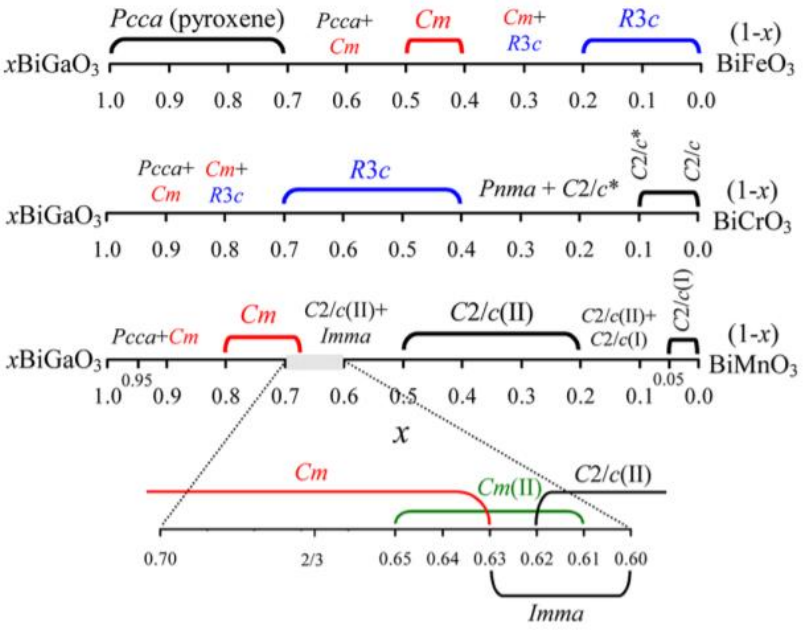

Figure 1-12 Structural phase diagrams for $BiGa_xM_{1-x}O_3$ (M=Cr, Mn, and Fe). *R*3*c* phase is a polar rhombohedral pervskite phase, *Cm* phase is the polar monoclinic perovskite phase with a giant *c*/*a* ratio, *C*2/*c* and *Imma* phases are non-polar monoclinic phase and orthorhombic phase, respectively, and *Pcca* phase is pyroxene phase. Reprinted with permission from [39]. Copyright 2016 American Chemical Society

1.3 Multiferroic materials for low energy consumption memory applications

Multiferroic materials are defined as materials which possess more than one ferroic orders such as ferroelectric and (anti)ferromagnetic orders simultaneously [42]. In the materials with a strong magnetoelectric coupling between magnetic and ferroelectric orders, it might be possible to manipulate magnetization by electric-field or the polarization by magnetic-field. Magnetization manipulation by electric-field is one of the ultimate goals for low-energy memory applications because it does not cause an energy loss by electric current flow [43]. Although a room temperature multiferroic material with the strong magnetoelectric coupling is required for the practical use, unfortunately, there was no report of such materials satisfying the severe requirements.

$TbMnO_3$ is one of the most well-known multiferroic material [44]. The material is a member of the perovskite $LnMnO_3$ family (*Ln*= lanthanide) which is known as parent compound of colossal magnetoresistive manganite $(Ln,Sr)MnO_3$ [45]. Perovskite $LnMnO_3$ has a rich magnetic phase diagram, which results from a magnetic frustration between the nearest-neighbor and the next-nearest-neighbor Mn spins [46,47]. $TbMnO_3$ has a cycloidal spin order in the *bc*-plane below 28 K, accompanied by an appearance of an electric polarization along the *c*-axis[48,49]. This material received remarkable attention because of the large magnetoelectric effect: the manipulation of the ferroelectric transition temperature and the polarization flip by applied magnetic field and so on[50].

Recently, magnetization switching by electric field was demonstrated in orthorhombic perovskite $(Dy,Tb)FeO_3$[51]. Although this material basically has an antiferromagnetic order, the rotation of the octahedra leads to a spin canting in the Fe site with a spontaneous weak ferromagnetic moment along the *c*-axis. Below the ordering temperature of Dy/Tb spins, an electric polarization is generated along the *c*-axis. This electric polarization originates from the displacement of Dy/Tb cation induced by the magnetic exchange interaction between Dy/Tb and Fe spins. This is known as an exchange striction. The magnetization can be reversed by electric polarization switching when the speed of electric field sweep is fast. The problematic point in this material is the very low ferroelectric transition temperature (~ 2.5 K), therefore it is impossible to use this material for memory device.

Rhombohedral perovskite $BiFeO_3$ (BFO) is one of the most promising multiferroic materials for room-temperature multiferroic memory applications[1]. This material has a high ferroelectric Curie temperature (T_C) ~1100 K and a high antiferromagnetic Néel temperature (T_N) ~600 K. Although this material has an antiferromagnetic order without net spontaneous magnetization because of the presence of a superimposed cycloidal spin modulation similar to that of $TbMnO_3$, the modulation can be suppressed by applying

external magnetic field or chemical substitution or epitaxial strain in thin films, accompanied by an appearance of a weak ferromagnetic moment [10,52-55]. The ferromagnetic spontaneous moment is generated by Dzyaloshinskii-Moriya (DM) interaction and is governed by the rotation of FeO_6 octahedra [56]. Recently, it was revealed that an electric polarization switching caused a change in octahedral rotation [8]. Therefore, we expect that the weak ferromagnetic moment can be controlled by a polarization switching in this material. Although many reports about the magnetization control by electric field in $BiFeO_3$ have been published, there is no report that the net ferromagnetic moment of $BiFeO_3$ is unambiguously changed by the polarization switching. J. T. Heron *et al*. demonstrated that an in-plane magnetization of CoFe upper layer was reversed by a polarization switching of a BFO thin film in $CoFe/BiFeO_3/SrRuO_3/DyScO_3$ heterostructure, clearly indicating that the polarization switching of $BiFeO_3$ influence the magnetic properties of CoFe layer[8]. However, the switching of the weak ferromagnetic moment of BFO was not evident. Moreover, the presence of CoFe layer complicates the interpretation of the experimental results. A single-phase multiferroic material with ferroelectric and ferromagnetic order is therefore essential to study the intrinsic DM coupling between the two orders.

Our group has found that partial substitution of Co for Fe stabilized the collinear phase with weak ferromagnetism preserving the *R*3*c* crystal structure up to $x = 0.20$ for $BiFe_{1-x}Co_xO_3$ as shown in Fig. 1-13 and 1-14 [10,33,54]. It has been confirmed that the collinear phase possesses a net ferromagnetic component at room-temperature for $x = 0.10\sim0.20$. Therefore, $BiFe_{1-x}Co_xO_3$ ($x = 0.10$-0.20) is a single phase ferroelectric ferromagnetic material at room-temperature. We have confirmed the reorientation of the magnetic easy plane after electric poling though the remnant magnetization measurements on single crystals [11]. However, the complex domain structure in single crystals prohibited us from direct observation of local magnetization reversal by a polarization switching. It is supposed that epitaxial thin film sample is suitable to examination of the local change in ferroelectric/ferromagnetic domains because piezoelectric force and magnetic force microscopies can be utilized in epitaxial thin film sample: Both methods are surface sensitive technique and suitable for observation of the ferroelectric and magnetic domain structures.

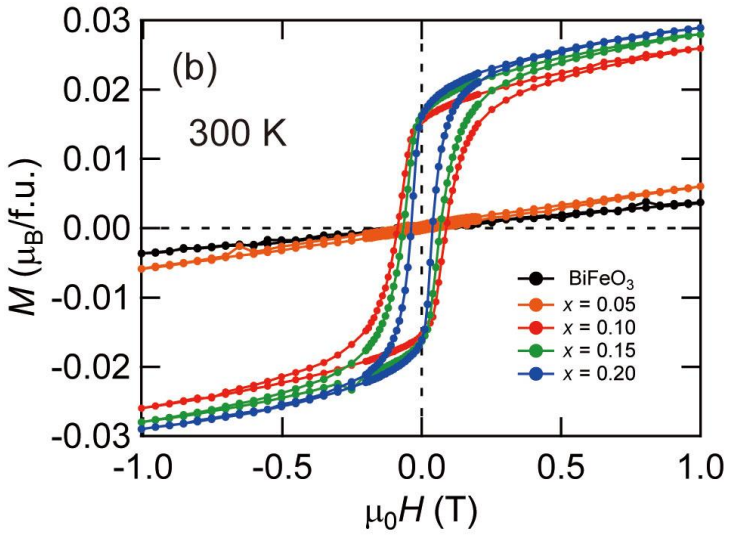

Figure 1-13 Magnetization vs magnetic field curves for $BiFe_{1-x}Co_xO_3$ powder samples at room-temperature. Ferromagnetic behavior is clearly observed for x = 0.10, 0.15, and 0.20 [11].

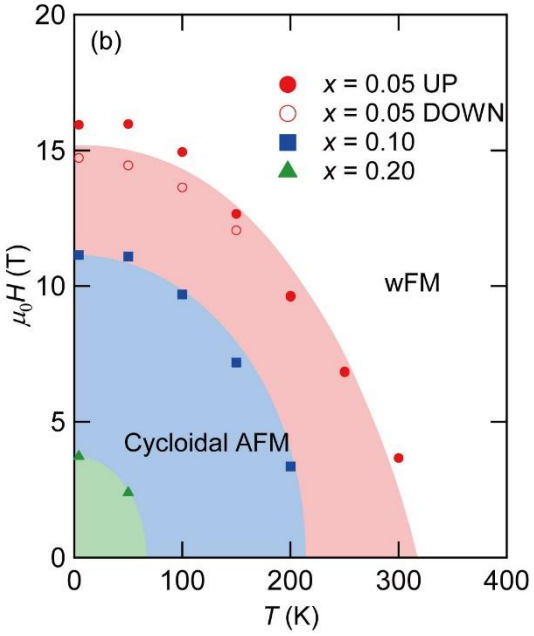

Figure 1-14 Magnetic phase diagram of $BiFe_{1-x}Co_xO_3$. Colored regions correspond to cycloidal spin phase. We clearly see that Co substitution for Fe drastically stabilize the collinear phase with a ferromagnetic moment [11].

1.4 The objective of this thesis

In this thesis, piezoelectric and multiferroic properties of $BiFeO_3$-based thin films are studied. The objective of this thesis is to reveal a capability of Bi-containing perovskite oxide as advanced functional electric materials.

First, I attempted to demonstrate a piezoelectric response enhancement due to polarization rotation in Bi-containing perovskite oxides. Bi-containing perovskite oxides is expected to be a candidate for replacing PZT, but the piezoelectric response is much lower than that of PZT. Therefore, the improvement of the piezoelectric response is required, A polarization rotation as observed in the monoclinic PZT is considered to be a key factor to improve the piezoelectric response of Bi-based lead-free piezoelectric material. In this thesis, $BiFe_{1-x}Co_xO_3$ and $BiFe_{1-x}Ga_xO_3$ are selected as research targets because both material has a monoclinic phase with a giant *c*/*a* ratio the same as the monoclinic PZT. Additionally, the orientation dependence of the piezoelectric properties of the monoclinic $BiFe_{1-x}Ga_xO_3$ is also examined.

Second, I attempted to directly observe the magnetization reversal by electric field and to elucidate the switching mechanism of $BiFeO_3$-based multiferroic materials. Although $BiFeO_3$ has an antiferromagnetic order without net spontaneous magnetization at room temperature, external stimuli such as strong magnetic field or epitaxial strain or Co-substitution induces a ferromagnetic moment due to spin canting by Dzyaloshinskii-Moriya (DM) interaction. Although the moment was anticipated to be controlled by the electric polarization switching, the direct observation was absent. In this thesis, a detailed switching mechanism of the magnetization reversal is elucidated in single phase ferromagnetic ferroelectric Co-substituted $BiFeO_3$ thin films.

The outline of this thesis is as follows.

In the chapter 2, enhancement of the piezoelectric properties of $BiFe_{1-x}Co_xO_3$ thin films with a giant *c*/*a* ratio are demonstrated.

In the chapter 3, the piezoelectric response and its orientation dependence of $BiFe_{1-x}Ga_xO_3$ thin films with a giant *c*/*a* ratio are examined.

In the chapter 4, a magnetization reversal by electric field in $BiFe_{1-x}Co_xO_3$ thin film is demonstrated and the mechanism is discussed.

In the chapter 5, conclusion and future perspectives are given.

Chapter 2

Enhanced piezoelectric response due to a polarization rotation in $BiFe_{1-x}Co_xO_3$ thin films with a giant *c*/*a* ratio*

2.1 Introduction

Perovskite compound $PbZr_{1-x}Ti_xO_3$ (PZT) is most widely used because of its large piezoelectric constant and high-temperature stability. PZT shows a maximum piezoelectric response at a compositional phase boundary ($x \approx 0.48$), a so-called morphotropic phase boundary (MPB), between rhombohedral (space group (SG); *R*3*m*) and tetragonal (SG; *P*4*mm*) phases [14]. The enhanced piezoelectric properties of PZT at the MPB are generally attributed to the presence of a monoclinic phase (SG; *Cm*) [15,57] (designated as M_A -type by Vanderbilt and Cohen) [19], where the polarization direction can rotate between [001] and [111] (in pseudo-cubic notation) because of a lack of a symmetry axis. This leads to an enhanced piezoelectric response to the applied electric field and stress [17,18,58].

Although the polarization rotation mechanism successfully explains the enhanced piezoelectric response of PZT at the MPB, the presence of the monoclinic phase as a distinct phase is still in dispute [59-61]. Nano-sized domains of tetragonal and/or rhombohedral phases, which show up as a monoclinic phase in the diffraction pattern, can be the origin of the enhanced piezoelectric response due to the flexibility to the applied electric field and stress. The small structural differences between tetragonal, rhombohedral, and monoclinic phases inhibit the structural analysis and make it difficult to elucidate the key factor in the enhanced piezoelectric response of PZT at the MPB. In this regard, we have discovered the same M_A-type monoclinic phase as the PZT at the MPB as a distinct phase in the solid solution between rhombohedral (SG; *R*3*c*) $BiFeO_3$ (BFO) [1] and tetragonal (SG; *P*4*mm*) $BiCoO_3$ [5], $BiFe_{1-x}Co_xO_3$ (BFCO) [33], at $x \approx 0.3$. Furthermore, the polarization rotation between [001] and [111] was observed as

---

* This work is published in [91]. K. Shimizu et al., "Enhanced Piezoelectric Response due to Polarization Rotation in Cobalt-Substituted $BiFeO_3$ Epitaxial Thin Films." Advanced Materials 28, 8639 (2016).

functions of temperature and composition [34] in powder X-ray diffraction (XRD). Because the monoclinic phase has a giant *c*/*a* ratio (≈1.26) originating from $BiCoO_3$, the M_A-type monoclinic phase is identified without ambiguity. Therefore, the monoclinic BFCO is an ideal material with which to study the role of the polarization rotation in piezoelectric materials. However, high leakage current presumably at grain boundaries has prevented us from evaluating the piezoelectric properties in a ceramic form. Thin film samples are indispensable to evaluate the piezoelectric properties of monoclinic BFCO.

There have been many publications on the fabrication of BFO thin films and their ferroelectric/piezoelectric properties since the first report by Wang *et al.* [6]. M_A-type monoclinic structure is generally observed for BFO thin films on substrates with moderate lattice mismatch [62]. Note that the *c*/*a* ratio of this structure is close to unity (≈1.02), and this structure is different from that of the M_A-type monoclinic BFCO with a giant *c*/*a* ratio. When fabricated on substrates with compressive strain over 4.5% such as $LaAlO_3$ (LAO) (001), BFO thin films with a giant *c*/*a* ratio (≈1.23) are stabilized [40,41]. This phase, later identified as M_C -type monoclinic structure [63,64], is similar to the M_A-type monoclinic BFCO but is different in that the polarization tilts toward [101] instead of [111]. Recently, M_A-type monoclinic structure with a giant *c*/*a* ratio was realized for $BiFe_{0.6}Ga_{0.4}O_3$ in the form of thin films [65], but the piezoelectric property of which is yet to be reported. Concerning the piezoelectric properties of the BFO thin films, it was demonstrated that an electric-field-induced transformation from a paraelectric orthorhombic phase to the polar rhombohedral phase is the origin of enhanced piezoelectric coefficient in rare-earth substituted BFO thin films [27,66]. Nanodomains found in these films also support this picture [67]. However, there have been no experimental reports that discussed the role of electric-field induced polarization rotation as the origin of the enhanced piezoresponses.

In this chapter, epitaxial BFCO (x = 0–0.50) thin films with M_C-type, M_A-type monoclinic structures and tetragonal structure were prepared on (001)-oriented $LaAlO_3$ (LAO) substrates, and their structural and piezoelectric properties were investigated to demonstrate enhancing the piezoelectric response by introducing polarization rotation.

2.2 Experiment

BFCO thin films were prepared using pulsed laser deposition (PLD) with a KrF excimer laser (λ = 248 nm). PLD is categorized as physical vapor deposition (PVD) process. The thin films samples were prepared by using pulsed laser deposition method (PLD). PLD is categorized as physical vapor deposition (PVD) process. A pulsed laser is focused onto a ceramics target mounted in a vacuum chamber. Then, ablated plume from the target deposits on a substrate as thin film. The advantages of PLD are stoichiometric transfer from target to thin film and an abundance of growth parameters, which enables to grow high quality thin films with a complicated composition, such as perovskite oxides thin films. Schematic illustration of PLD system is shown in Fig. 2-1. A pulsed laser was focused on targets with an energy density of 1.5 J/cm^2. The composition of the targets was stoichiometric at a cation ratio. During the deposition, the substrate temperature was kept at 630–680 °C in an oxygen partial pressure of 17 Pa. The thicknesses of all thin films were fixed at 90–100 nm as determined by cross-sectional field-emission scanning electron microscope (SEM; JEOL JSM-6610) observation. A $La_{0.5}Sr_{0.5}CoO_3$ (LSCO) layer with a thickness of 30 nm was deposited as a bottom electrode for piezoelectric measurements. The crystal structure of the thin films was investigated by XRD with Cu Kα radiation (Rigaku SmartLab) and by scanning transmission electron microscope (STEM, JEOL ARM-200F) using a system equipped with a HAADF detector. Surface topography images were taken on an atomic micro scope (AFM, Agilent 5420) in contact mode. Local piezoelectric strain versus electric field curves were measured by detecting the vertical motion of an AFM cantilever with a conducting tip connected to a ferroelectric test system (Toyo FCE-1E)

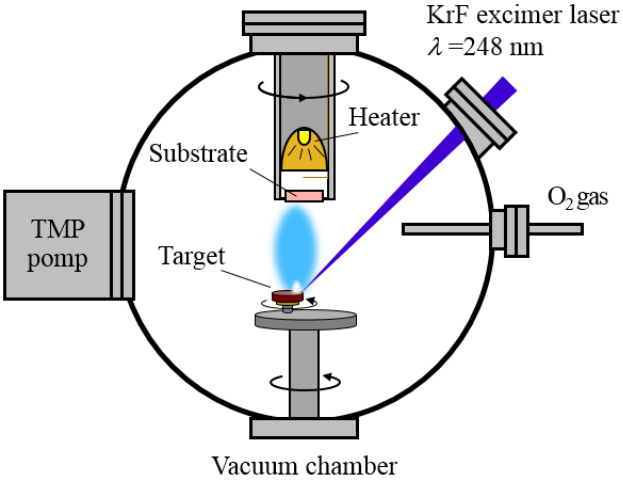

Figure 2-1 The schematics illustration of PLD system

2.3 Results and discussion

2.3.1 Crystal structure

Figure 2-2a shows the θ–2θ XRD patterns of BFCO thin films. The thin films were found to be *c*-axis oriented without detectable impurity phases for all compositions. The calculated out-of-plane lattice constants are 4.66–4.70 Å. Figure 2-2b shows a cross-sectional high-angle annular dark-field scanning transmission electron microscopy (HAADF STEM) image of a x = 0.30 BFCO thin film. The c/a ratio estimated from the atomic positions is ≈1.2–1.3. These results show that all the BFCO thin films have a giant c/a ratio (1.2–1.3).

Reciprocal space mapping (RSM) around 103 and 113 reflections of LAO was performed to investigate the detailed crystal structure further. The RSMs for the BFCO thin films with x = 0.10, 0.15, 0.30, and 0.50 are shown in Figure 2-3a as representative results. At x = 0–0.10, the 103 reflections of BFCO split into three spots, while the 113 reflections split into two spots, indicating that the crystal structure is an M_C–type monoclinic one, as schematically illustrated in Figure 2-3b. This structure is identical to that of the aforementioned M_C-type BFO thin films with a giant c/a ratio. However, at x = 0.20–0.30, the 103 reflections of BFCO split into two spots, while the 113 reflections split into three spots. This result indicates that the structure changed to an M_A-type monoclinic structure (Figure 2-3c), which is the same as the bulk monoclinic BFCO at the MPB. Note that M_A and M_C-type monoclinic phases coexist at x = 0.15. The crystal structure becomes $BiCoO_3$-type tetragonal at x = 0.5 (Figure 2-3d) as is evident from the absence of peak splitting in both the 103 and 113 reflections. Thus, the crystal structure of BFCO thin films undergoes successive transitions from M_C-type to M_A-type monoclinic phases and finally to a tetragonal phase as Co content x increases.

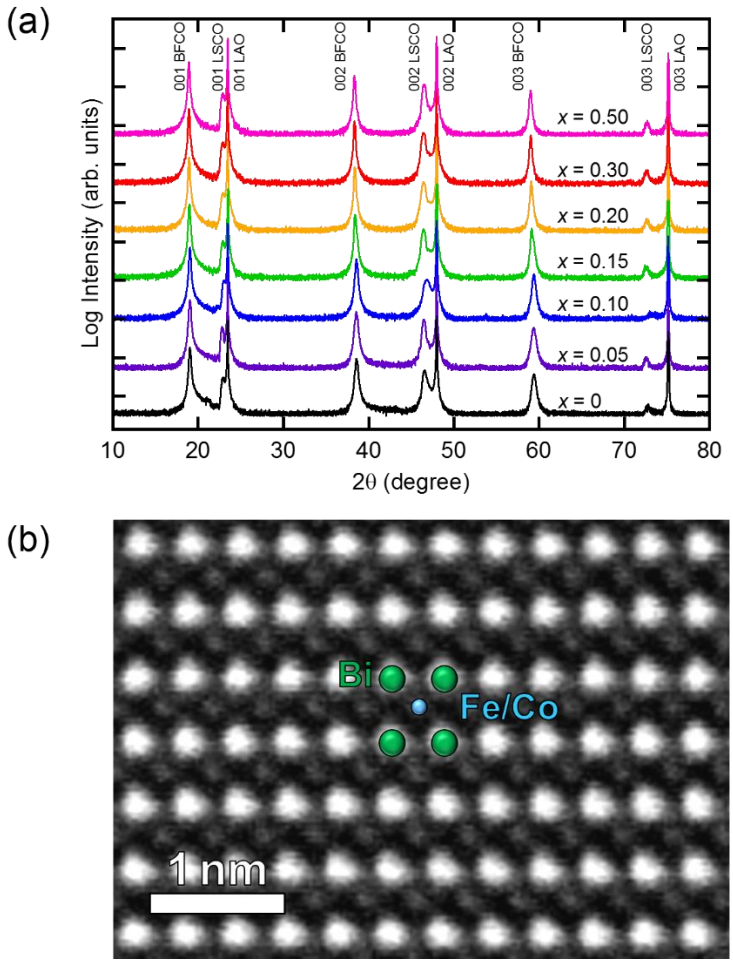

Figure 2-2. a) XRD θ–2θ patterns of BFCO thin films. All the films are c –axis oriented without detectable impurity phases. b) Cross-sectional HAADF STEM image of x = 0.30 BFCO thin film. It can be clearly seen that the BFCO thin film has a giant c/a ratio of 1.2–1.3.

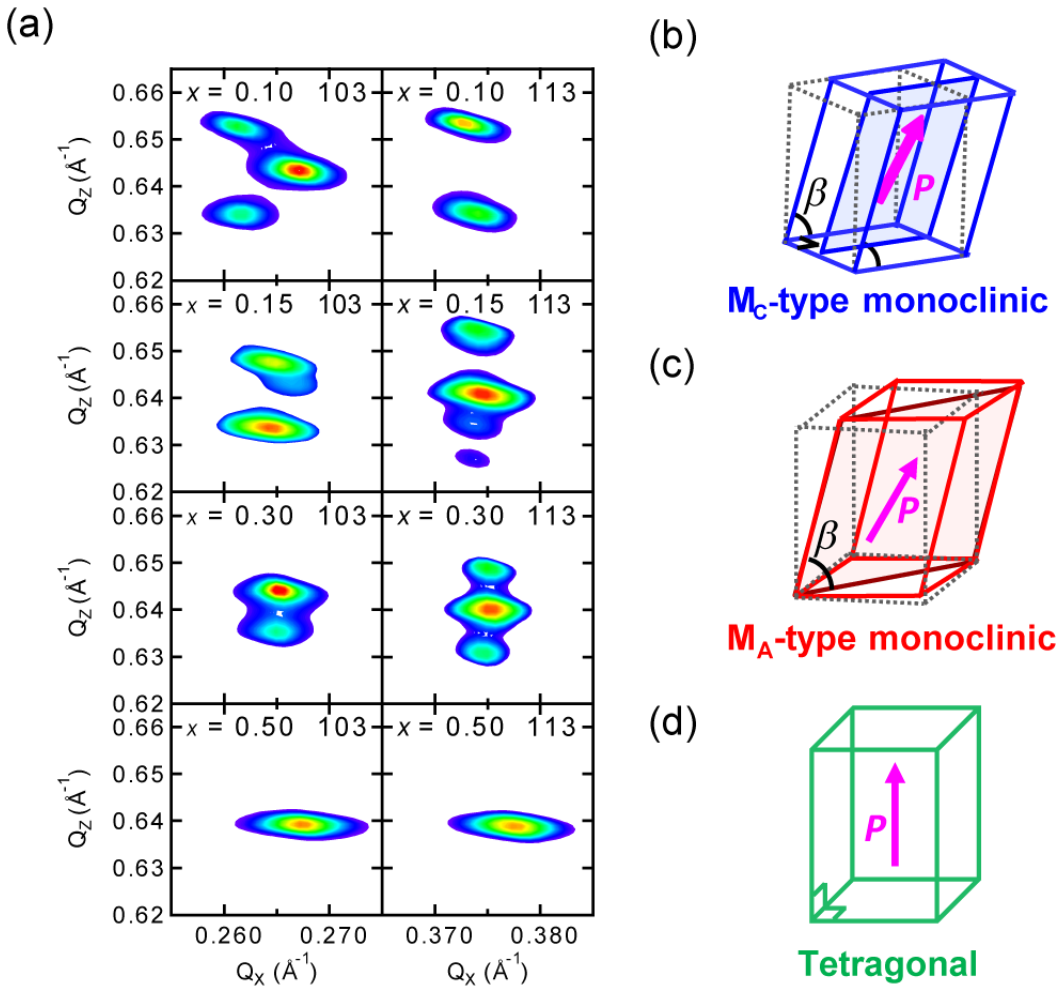

Figure 2-3. a) Reciprocal space mapping around 103 and 113 LAO for BFCO thin films with x = 0.10, 0.15, 0.30, and 0.50. Schematic illustrations of b) M_C-type monoclinic, c) M_A–type monoclinic, and d) tetragonal structures. Note that the polarization tilts toward [101] and [111] in the M_C-type and M_A-type monoclinic structures, respectively

The lattice parameters were calculated from RSM data and are plotted in Figure 2-4 as functions of composition. Because lattice parameters show different dependence on x in M_C-type and M_A -type regions, they are discussed separately. In the M_C-type monoclinic region (x = 0–0.10), the out-of-plane lattice parameter c decreases as x increases, while the in-plane lattice parameters a_{pc} and b_{pc} increase, and the average of these approaches the pseudo-cubic lattice parameter of LAO substrates (≈3.79 Å). This behavior is contrary to my expectation because BCO has smaller in-plane and larger out-of-plane lattice constants compared to M_C-type monoclinic BFO, indicating that larger tensile strain is imposed on the BFCO thin films as x increases. It can be explained by the fact that the fraction of a "rhombohedral-like phase" decrease, which is noticeable in atomic force microscopy (AFM) images, as discussed in detail later. By further increasing x to 0.15, an M_A-type monoclinic phase starts to appear. The lattice parameter c increases abruptly when the structure changes from M_C to M_A-type monoclinic phases, indicating that this structural phase transition is of the first order. Note that only the lattice parameters of the M_A-type monoclinic phase are plotted in Figure 2-4 for x = 0.15 BFCO because RSM reflections from the M_C-type monoclinic phase were too weak to locate them correctly. However, the lattice parameters of the M_A phase gradually approach those of the tetragonal phase as x increases in a second-order manner. Such behavior is consistent with those of bulk BFCO, again demonstrating that the M_A-type monoclinic phase is essentially the same as the bulk BFCO with a giant c/a ratio.

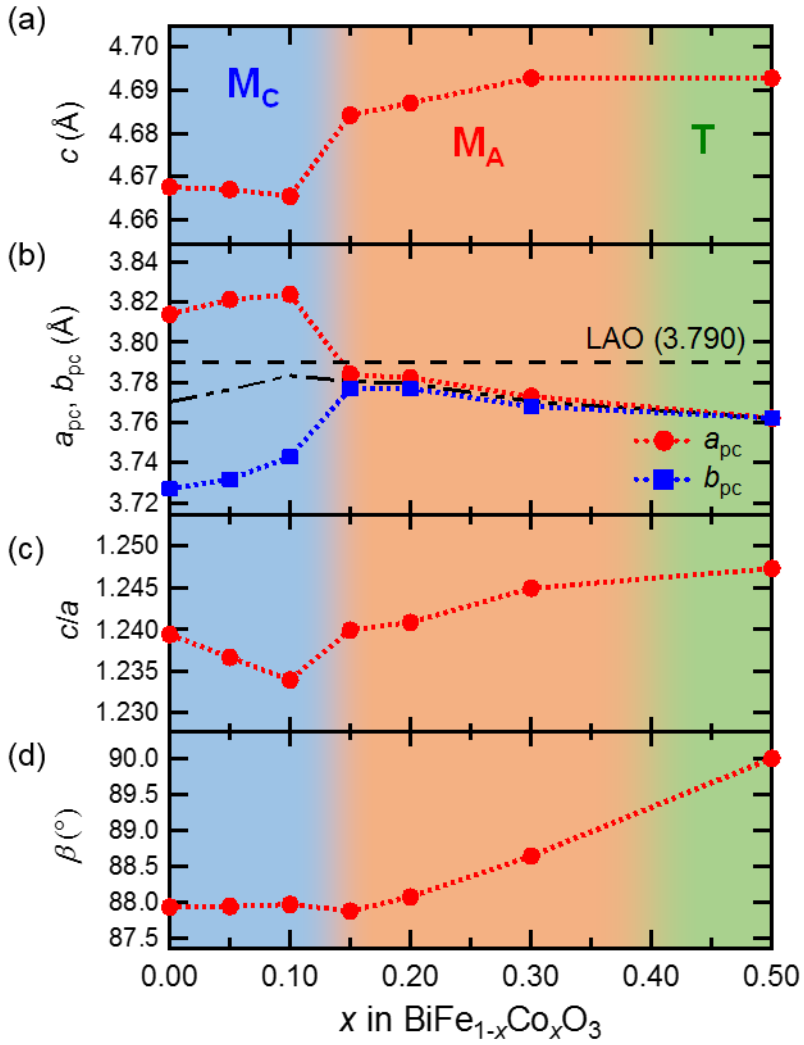

Figure 2-4. a) Out-of-plane lattice parameter c, b) in-plane lattice parameters a_{pc} and b_{pc}, c) c/a ratio, and d) monoclinic β angle as obtained from RSMs through the BFCO peaks as function of cobalt content x. The structures of the different phases are indicated. The unit cell is defined as $a_{pc} \times b_{pc} \times c_{pc}$ and $\sqrt{2}\ a_{pc} \times \sqrt{2}\ b_{pc} \times c_{pc}$ in the M_C-type and M_A–type monoclinic phases, respectively [68,69].

2.3.2 Domain structure

Figure 2-5 shows AFM images of BFCO thin films with x = 0.05, 0.10, 0.30, and 0.50. All the films are basically flat except for a striped contrast and long-valley-like contrasts observed in M_C-type (Figure 2-5a,b) and M_A-type (Figure 2-5d,e) monoclinic phases, respectively. The striped area is generally observed in BFO thin films on LAO substrates thicker than 50 nm and is attributed to the area where the M_C-type monoclinic phase and rhombohedral-like phase coexist [27]. This rhombohedral-like phase is introduced to accommodate the lattice mismatch between M_C-type monoclinic BFO films and the substrate. It can be clearly seen that the striped area decreases as x increases. This means the fraction of the rhombohedral-like phase decreases as x increases, as is naturally expected from the phase diagram of bulk BFCO [13]. This is why larger tensile strains are imposed on the BFCO thin films in the M_C-type monoclinic region as x increases (Figure 2-4a,b). However, the long-valley-like contrast in the M_A-type phase is different from the striped contrast observed in the M_C-type phase samples. A cross-sectional HAADF STEM observation was conducted to clarify the origin of such contrast. Figure2-5f shows an HAADF STEM image of x = 0.30 BFCO thin film at the area where long-valley-like contrast exists. The existence of "90° domains" where neighboring domains share 101} planes is clear. The angle between the c -axis orientated domain (the so-called c-domain) and the domain sandwiched in c -domains, the so-called a-domain, is ≈51°, which is consistent with that expected from the c/a ratio of the film (arctan (c/a) = arctan (1.244) = 51.2°). The width of the a-domain is as narrow as ≈ 2 nm (≈6 u.c.). The "averaged" in-plane lattice parameter of BFCO thin film was roughly calculated to be 0.379 nm assuming that the widths of c-domains and a–domains are ≈1 μm and 6 × 0.47 nm, respectively. Interestingly, this is identical to the lattice parameter of LAO, indicating that the a-domain, hence the long-valley-like structure, is introduced to relieve the lattice mismatch between BFCO thin films and the LAO substrates. This assertion is supported by the fact that the density of the long-valley-like contrast increases as x increases from x = 0.15 to 0.50 (Figure 2-5c–e), which corresponds to the increase in the lattice mismatch between BFCO thin films and LAO substrates (Figure 2-4b). Importantly, because the piezoelectric measurements presented in the next paragraph were locally performed at the flat surface area of the BFCO thin films, the observed piezoelectric response should be intrinsic properties of BFCO thin films that are related to the crystal structure and presence or absence of polarization rotation and not extrinsic effects such as domain switching from rhombohedral-like phases (x = 0–0.10) or a-domains (x = 0.20–0.50) to possibly tetragonal-like phases. Note that twinning is present in the LAO substrates used in this study. When the scan area of AFM is larger (e.g., 50 μm × 50 μm), we sometimes

see the contrast due to twinned domain boundary. However, the size of domains is much larger than the scan area of the AFM images (3 μm × 3 μm), and the AFM images shown in Figure 2-5 do not include the twin domain boundary. The AFM images and piezoelectric responses shown later are reproducible at different twinned domains within the experimental error.

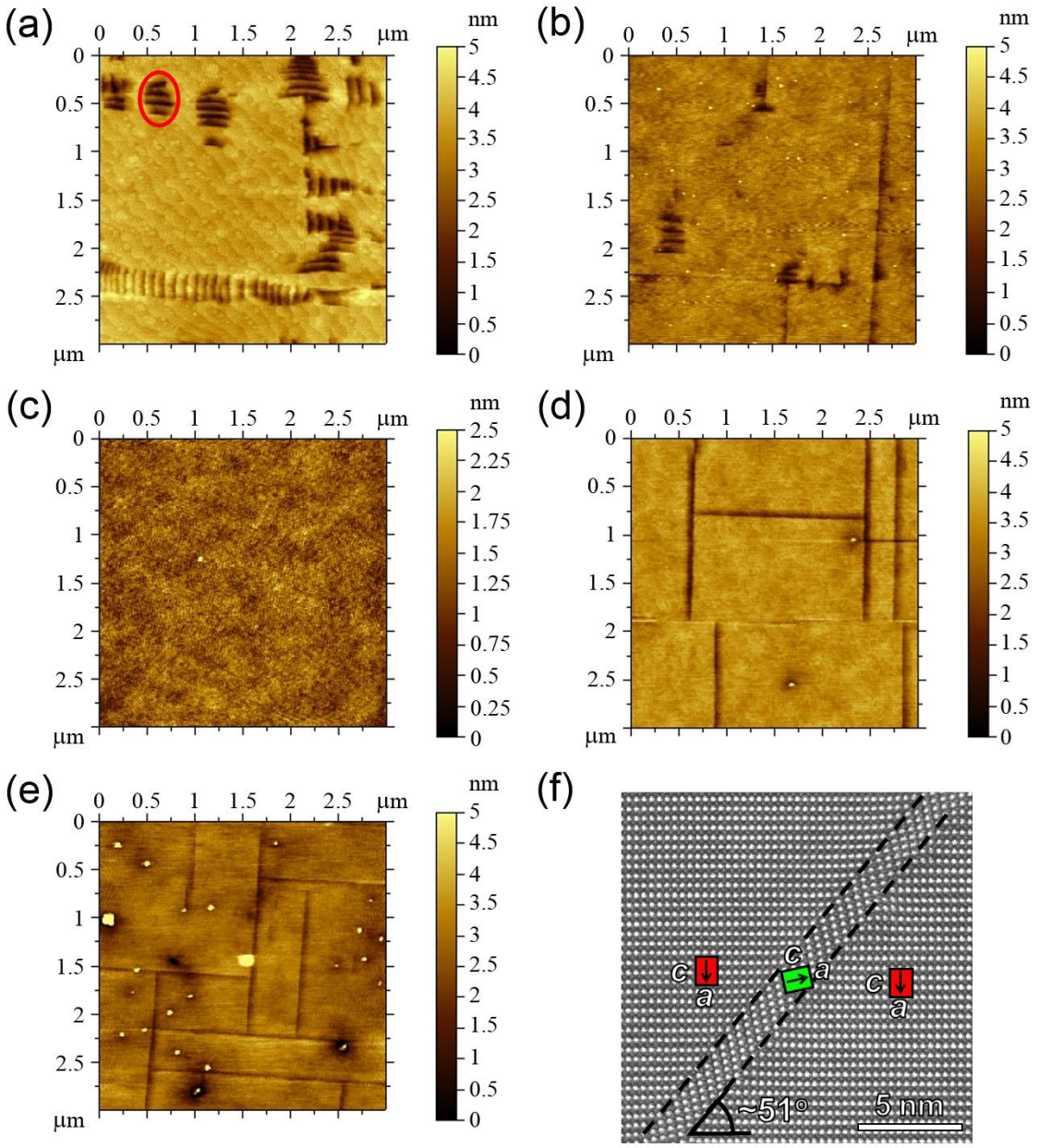

Figure 2-5. AFM topography images of BFCO thin films with a) x = 0.05, b) x = 0.10, c) x = 0.15, d) x = 0.30, and e) x = 0.50. Scan size is 3 µm for all images. The striped area marked with the red circle decreases in the M_C-type monoclinic phase as x increases from 0.05 to 0.15. Long-valley-like contrasts appear in the M_A-type monoclinic phase, the density of which decreases as x decreases. f) Cross-sectional HAADF STEM image of x = 0.30 thin film covering the area where long-valley-like contrast exists.

2.3.3 Piezoelectric properties

Because M_C-type, M_A-type monoclinic, and tetragonal phases were successfully stabilized, the piezoelectric properties of these thin films were investigated. Unipolar ac electrical fields at a frequency of 1 kHz and a bias of ~880 kV/cm were applied directly on bare BFCO thin films from a conductive cantilever. Figure 2-6a shows local piezoelectric strain versus electric field (*S*–*E*) curves for BFCO thin films. I also tried a bipolar electrical field for the *S*–*E* measurements, but it was not successful most probably because of a built-in potential that aligns the polarization downward [70] and also because of a large coercive field. The *S*–*E* curves of monoclinic phases (x = 0–0.30) show a nonlinear dependence on the electric field. The effective piezoelectric constant S_{MAX}/E_{MAX} calculated from the *S*–*E* curves is plotted in Figure 2-6b. The S_{MAX}/E_{MAX} value decreases from 39.8 to 36.3 pm/V as Co content x increases in the M_C structure, presumably reflecting the enhanced tensile strain imposed by the substrates. These values are comparable to that of a former report (~30 pm/V) on M_C-type BFO thin films [71]. The S_{MAX}/E_{MAX} value increases from 52.1 to 57.5 pm/V in the M_A structure. Interestingly, the maximum value was obtained at x = 0.20 rather than at x = 0.15, which is the MPB composition between M_C and M_A phases. This means that the enhanced piezoelectric responses were achieved in a single phase of the M_A. The S_{MAX}/E_{MAX} value in the tetragonal phase (x = 0.50) is as small as 10.8 pm/V. Our study clearly demonstrates that a piezoelectric response is enhanced in the monoclinic phases due to the polarization rotation and that polarization can rotate more easily in the M_A phase than in the M_C phase, which is consistent with the prediction by Fu and Cohen based on first-principles calculations[16]. Moreover, when comparing β angles and S_{MAX}/E_{MAX} values of x = 0.20, 0.30, and 0.50 BFCO thin films, one can notice that a larger deviation in the β angle from 90° leads to an enhanced piezoelectric response. This should be related to the fact that BFCO thin films with a smaller β angle have more room for polarization to rotate. The reason that x = 0.15 BFCO thin film, which has the smallest β angle, shows smaller piezoelectric response than x = 0.20 BFCO thin film, should be attributed to the coexistence of the M_C phase, which has smaller piezoresponse than the M_A phase. Note again that because the piezoelectric measurements were locally performed at the *c*-domain region, we can exclude the extrinsic effects such as domain switching from rhombohedral-like phases (x = 0–0.10) or *a*-domains (x = 0.20–0.5) to *c*-domains as the origin of enhanced piezoelectric responses in these films. Besides, because the *c*/*a* ratio of M_C phase is smaller than that of M_A phase, electric field induced transition from M_A to M_C phase is not likely. Instead, transition from M_A to tetragonal phase can happen considering the structural continuity between M_A phase and the tetragonal phase, which

can be regarded as polarization rotation. The origin of the dependence of *S*–*E* curves on the nonlinear field in the monoclinic phases is not clear. However, considering the small difference in crystal structure between M_A-type monoclinic and tetragonal phases, and only the latter show linear *S*–*E* curves, it should be the intrinsic properties of the monoclinic phase which is related to polarization rotation rather than extrinsic effects such as the electrostriction effect. It should be noted that the piezoelectric responses of my BFCO thin films are much smaller than those of PZT and still smaller than those of BFCO on $SrTiO_3$(001) substrates [28]. This is probably due to the large spontaneous polarization of present BFCO thin films. Ionic model calculations based on the Rietveld refinement of the bulk crystal structure indicated the polarization of BFCO with $x = 0.30$ is 117 μC/cm^2 [34], while that of PZT at MPB composition is ≈37.6 μC/cm^2 [72]. Such a trend is also observed in our recent study on the crystal structure and piezoelectric properties of $Bi_2ZnTi_{0.6}Mn_{0.4}O_6$ bulk and thin film samples [73]. This behavior can be explained using a Landau–Ginzburg–Devonshire theory: piezoelectric coefficient comes from the product of dielectric constant and polarization, and dielectric constant decreases faster than polarization increases [25,74-76]. The M_A–type monoclinic phase with smaller spontaneous polarization and larger deviation in β angle from 90° would be desirable to achieve PZT replacement. Note that my conclusion does not exclude the phase coexistence regions at MPB in general piezoelectric materials as the origin of the piezoresponse enhancement. I expect that, when the polarization, hence the *c*/*a* ratio, is somehow reduced in the present material, the phase coexistence regions appear near MPB and superior dielectric/piezoelectric properties are realized.

2.4 Summary

Epitaxial BFCO thin films with a giant *c*/*a* ratio were successfully prepared. The crystal structure undergoes successive transitions from M_C-type monoclinic ($x = 0$–0.15) to M_A-type monoclinic phases ($x = 0.15$–0.30) and finally to a tetragonal phase ($x = 0.50$) as Co content *x* increases. The M_A phase is essentially the same as that found in bulk BFCO where polarization rotation has been found. Piezoelectric responses are enhanced in the monoclinic phases, especially in the M_A phase. A larger deviation in the β angle from 90° in the single M_A -type phase leads to enhanced piezoelectric response, which can be attributed to more room for polarization to rotate. These results provide a guideline for the further design and development of novel lead-free piezoelectric materials.

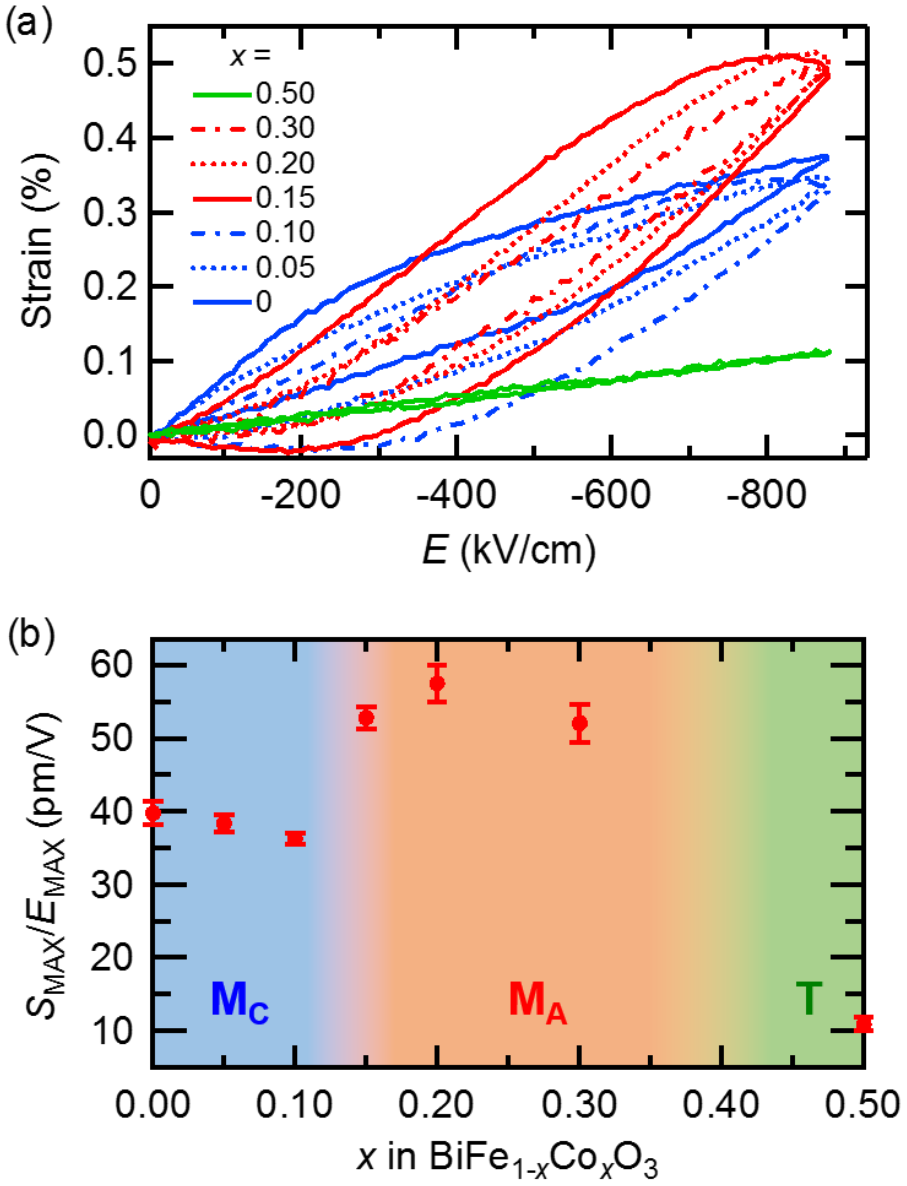

Figure 2-6. a) Local piezoelectric strain versus electric field curves for BFCO thin films. b) Effective piezoelectric constant S_{MAX}/E_{MAX} for BFCO thin films. The enhanced piezoelectric responses were achieved in a single phase of the M_A-type monoclinic structure with a larger deviation in β angle from 90°.

Chapter 3

Orientation control of piezoelectric properties of $BiFe_{1-x}Ga_xO_3$ thin films with a giant *c*/*a* ratio

3.1 Introduction

In the chapter 2, it was demonstrated that a M_A-type monoclinic phase in piezoelectric Bi-containing perovskite had an enhanced piezoelectric response due to a polarization rotation. Unfortunately, the piezoelectric response in $(001)_{pc}$-oriented monoclinic $BiFe_{1-x}Co_xO_3$ thin film with a giant *c*/*a* ratio was much smaller than that of PZT. In this chapter, $BiFe_{1-x}Ga_xO_3$ (BFGO) was chosen as next target of monoclinic lead-free piezoelectric material with polarization rotation. Furthermore, orientation dependence of piezoelectric response was investigated for further enhancement.

Since a monoclinic phase is generally considered to appear near the morphotropic phase boundary between rhombohedral and tetragonal phases, Bi-containing tetragonal perovskite is of great importance to produce a monoclinic phase. In 2005, P. Baettig *et al*. theoretically predicted that $BiGaO_3$ had a $PbTiO_3$-type tetragonal perovskite structure with a giant *c*/*a* ratio (~1.3) [77]. In 2006, A. Belik *et al*. succeeded in preparing $BiGaO_3$ by a high temperature high pressure method [3]. In contrast to the prediction, $BiGaO_3$ had a non-perovskite structure with GaO_4 tetrahedral coordination, known as pyroxene. Thereafter, H. Yusa *et al*. found that the pyroxene phase transformed into a perovskite phase under high pressure conditions above 3.2 GPa [38]. Up to 6.3 GPa, the perovskite phase keeps a M_A-type monoclinic phase (space group; *Cm*) with a giant *c*/*a* ratio the same as that of Co-substituted $BiFeO_3$ [34]. These results indicate that an enhanced piezoelectric response due to polarization rotation is also expected in this compound and its related solid solutions.

In 2012, A. Belik *et al*. successfully synthesized perovskite-type $BiGa_xM_{1-x}O_3$ (*M*=Cr, Mn, and Fe) by high temperature high pressure method [39]. They found that the M_A-type monoclinic phase with a giant *c*/*a* ratio appeared in all of these systems even under ambient pressure. It should be noted that the monoclinic phase in $BiFe_{1-x}Ga_xO_3$ can be stabilized at the lowest Ga content of $x = 0.30$~0.60 among them. Taking into account the fact that perovskite-type $BiGaO_3$ is unstable at ambient-pressure and $BiFeO_3$ is only simple Bi-based perovskite which can be prepared at ambient pressure, it is supposed that

BFGO thin films are relatively easy to obtain among above three systems. Indeed, Z. fan *et al*. succeeded in preparing the monoclinic $BiFe_{0.6}Ga_{0.4}O_3$ thin films [65]. Although the crystal structure and ferroelectric property of $BiFe_{0.6}Ga_{0.4}O_3$ thin film were investigated in the report, the description on the piezoelectric properties was absent. Besides, Ga content dependence of crystal structure was unclear.

The monoclinic phase with a giant *c*/*a* ratio has a highly anisotropic structure which enables polarization rotation. It is therefore expected to exhibit an unique orientation dependence of piezoelectric response. As shown by K. Oka *et al*., the lattice parameters *a* and *b* are more sensitive to polarization rotation by temperature and composition changes than the *c*-lattice parameter in the monoclinic BFCO, indicating that the piezoelectric constant related to the *a* and *b*-axes, such as d_{11}, d_{15}, and d_{24}, are expected to be higher than d_{33} [34]. These findings suggested that larger piezoelectric responses was expected in the monoclinic thin films with a giant *c*/*a* ratio in film orientations such as (110), (101). In this chapter, epitaxial $BiFe_{1-x}Ga_xO_3$ (BFGO) (x= 0-0.40) thin films are fabricated on $(001)_{pc}$ and $(110)_{pc}$ $LaAlO_3$ (LAO) substrates and the orientation dependence of piezoelectric properties are investigated.

3.2 Experiment

BFGO thin films were fabricated on $(001)_{pc}$ and $(110)_{pc}$-oriented $LaAlO_3$ (LAO) substrates using pulsed laser deposition with a KrF excimer laser ($\lambda = 248$ nm). A pulsed laser was focused on targets with an energy density of 1.5 J/cm^2. The composition of the targets was stoichiometric at a cation ratio. During the deposition, the substrate temperature was kept at 700–750 °C in an oxygen partial pressure of 17 Pa. The thicknesses of all thin films were fixed at 90–100 nm. A $La_{0.5}Sr_{0.5}CoO_3$ (LSCO) layer with a thickness of 30 nm was deposited as a bottom electrode for piezoelectric measurements. The crystal structure of the thin films was investigated by XRD with Cu Kα radiation (Rigaku SmartLab). Local piezoelectric strain versus electric field curves were measured by detecting the vertical motion of an AFM cantilever with a conducting tip connected to a ferroelectric test system (Toyo FCE-1E). Unipolar ac electrical fields at a frequency of 1 kHz and a bias of ~880-1000 kV/cm were applied directly on bare BFGO thin films from a conductive cantilever.

3.3 Results and discussion

3.3.1 Crystal structure

3.3.1.1Thin films on $(001)_{pc}$–oriented $LaAlO_3$ substrates

Figure 3-1 shows the θ–2θ XRD patterns of BFGO thin films. The thin films were found to be *c*-axis oriented for all compositions. The calculated out-of-plane lattice constants are 4.67–4.69 Å, indicating that all the BFGO thin films have giant *c*/*a* ratios (1.2–1.3).

Reciprocal space mapping (RSM) around 103 and 113 reflections of LAO was performed to further investigate the detailed crystal structure. Figure3-2 shows the RSMs for the BFGO thin films with x = 0, 0.20, and 0.40. At x = 0, the 103 and 113 reflections split into three and two spots, respectively, indicating that the crystal structure is an M_C–type monoclinic one. At x = 0.20, the 103 and 113 reflections split into two and three spots, respectively, indicating that the structure is an M_A-type monoclinic one. At x = 0.40, both reflections of BFGO split into three spots, indicating that the M_A and tetragonal phases coexist. The fraction of the tetragonal phase is roughly estimated to be 30% from the peak intensity ratio. The coexistence is not observed in BFGO bulk powder samples, where a tetragonal phase does not appear even up to 10 GPa [38,39]. Interestingly, the monoclinic distortion in the M_A phase of bulk powder samples gradually increases as Ga content increases in contrast to BFCO. It is suggested that the tetragonal phase in the thin film is stabilized by epitaxial strain or composition deviation such as oxygen or Bi deficiency.

The lattice parameters of the monoclinic phases calculated from RSM data are shown in Figure 3-3 as functions of composition. The *c* lattice parameter increases abruptly when the structure changes from M_C (x = 0) to M_A (x = 0.20, 0.40). The difference between the in-plane lattice parameters *a* and *b* is smaller in the M_A phase than in the M_C phase. These behaviors are the same as those of $BiFe_{1-x}Co_xO_3$ thin films as discussed in chapter 2. It is confirmed that the *c*/*a* ratio and the β angle in the M_A phase increases gradually as Ga content x increases.

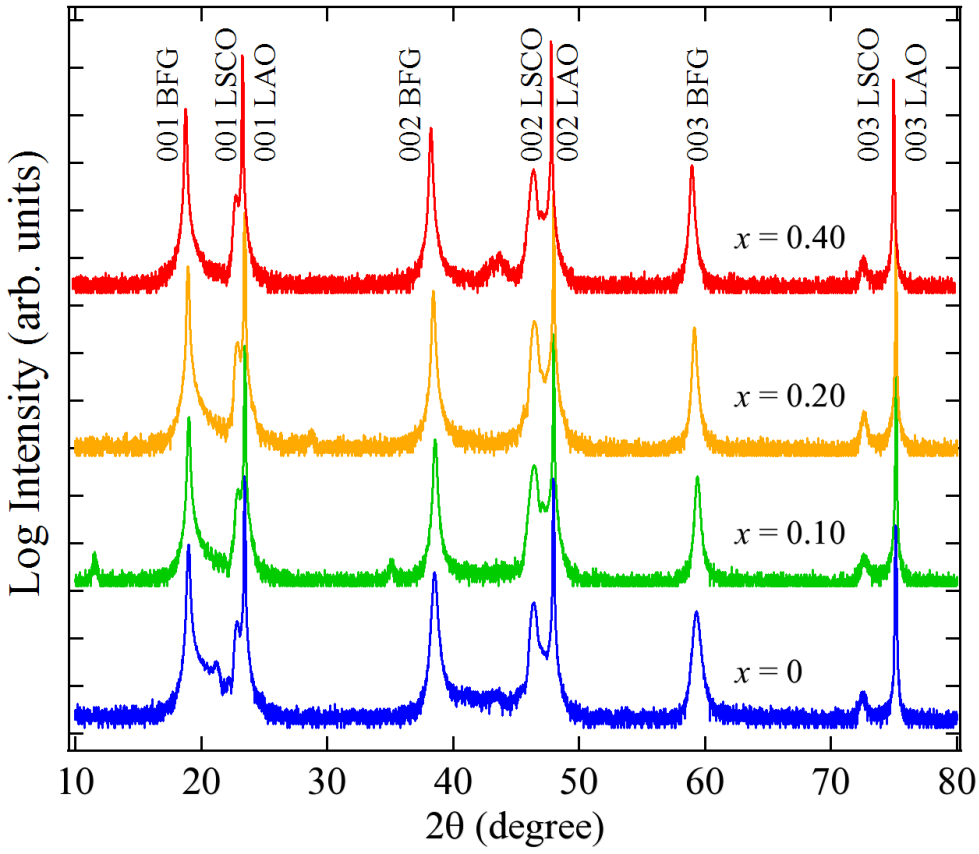

Figure 3-1. XRD θ–2θ patterns of BFGO thin films on $(001)_{pc}$-oriented LAO substrates. All the films are *c* –axis oriented.

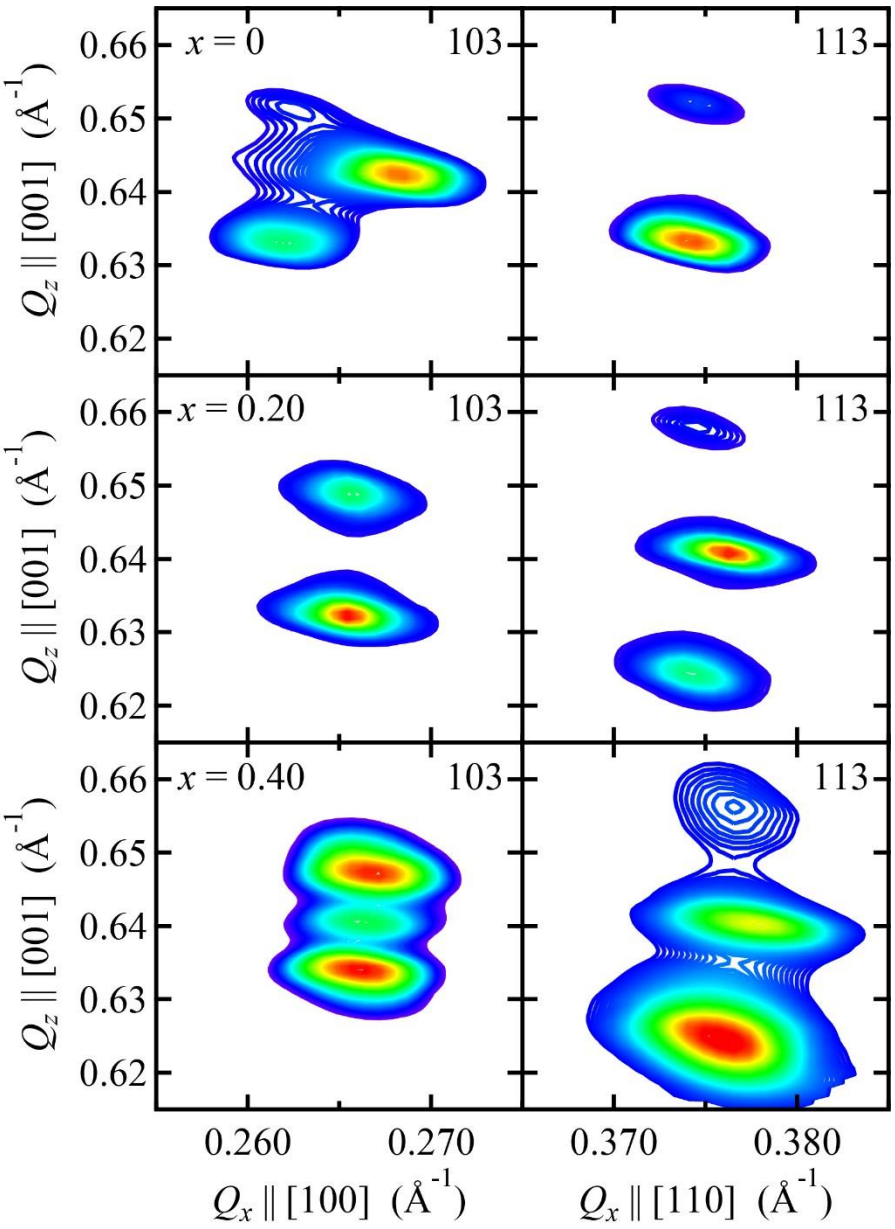

Figure 3-2. Reciprocal space mappings around 103 and 113 LAO for BFGO thin films on $(001)_{pc}$-oriented LAO substrates with x = 0.10, 0.20, and 0.40.

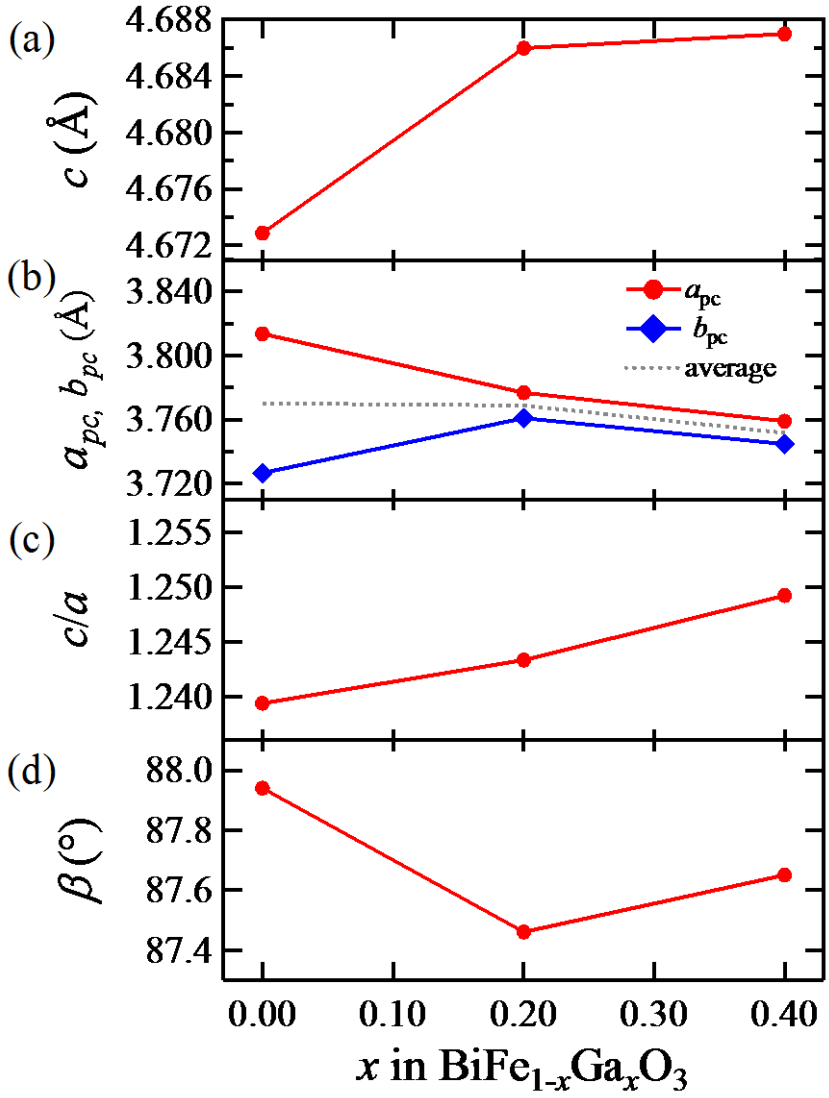

Figure 3-3. a) Out-of-plane lattice parameter c, b) in-plane lattice parameters a_{pc} and b_{pc}, c) c/a ratio, and d) monoclinic β angle of the monoclinic BFGO as obtained from RSMs through the BFGO peaks as function of Ga content x. The unit cell is defined as $a_{pc} \times b_{pc} \times c_{pc}$ and $\sqrt{2}\ a_{pc} \times \sqrt{2}\ b_{pc} \times c_{pc}$ in the M_C-type and M_A–type monoclinic phases, respectively.

3.3.1.2 Thin films on $(110)_{pc}$-oriented $LaAlO_3$ substrates

Figure 3-4 shows the θ–2θ XRD patterns of the BFGO thin films on $(110)_{pc}$ $LaAlO_3$ substrates. Although there is a small amount of impurity phase peaks, most of the observed peaks can be indexed assuming *h*0*h* perovskite peaks. The number of perovskite peaks of the BFGO (x = 0-0.40) thin films is one for x = 0, three for x = 0.10, 0.20, and two for x = 0.40, respectively. The three *d*-spacings are roughly estimated to be 2.83, 2.90, and 2.97 Å, as shown in Fig. 3-5. Calculated d_{101} and $d_{10\bar{1}}$ of rhombohedral $BiFeO_3$ are ~2.82 and 2.79 Å, and calculated d_{101} and d_{110} of tetragonal $BiCoO_3$, a representative tetragonal perovskite with a giant *c*/*a* ratio (hereinafter called GT phase), are ~2.93 Å and 2.64 Å, respectively. Therefore, it is concluded that all the BFGO thin films are $(101)_{pc}$-oriented and the phases in each films are as follows: only a rhombohedral phase (hereinafter called R phase) for x = 0, both R and GT phases for x = 0.10 and 0.20, and only a GT phase for x = 0.40. It was reported that $(101)_{pc}$-oriented pure $BiFeO_3$ thin film had a giant *c*/*a* ratio when the thickness was very thin (~10 nm) [78]. Since the GT phase can be prepared even in ~90-100 nm thick film, it is evident that a Ga-substitution for Fe greatly stabilizes the GT phase. The reported value of d_{101} in the BFO thin film is ~ 2.985 Å, which is almost identical to those of the present BFGO films. It should be noted that the peak of GT phase split into two, implying that the GT phase has a lower symmetry than tetragonal and is presumably monoclinic. Since the 101 peaks of a M_C phase and a M_A phase splits into three and two, respectively, the GT phase is more likely to be a M_A phase same as the bulk samples. The polarization direction inclines from the film normal, as shown in an inset of Fig. 3-4. Moreover, the out-of-plane $(101)_{pc}$ has the *a*-axis component, which is confirmed to be highly sensitive to polarization rotation in powder samples. Therefore, the film in this orientation is expected to exhibit higher piezoelectric response than that in the $(001)_{pc}$-orientation.

Reciprocal space mappings (RSMs) around 220 and 221 and 120 reflections of LAO were performed on the BFGO thin film with x = 0.40 to investigate the detailed crystal structure of the GT phase. $(110)_{pc}$-oriented LAO substrate has an in-plane 2-fold symmetry: the values of in-plane lattice parameter along $[001]_{pc}$ and $[\bar{1}10]_{pc}$ are $1 \times a_{pc}$ and $\sqrt{2} \times a_{pc}$, respectively (a_{pc} denotes pseudo-cubic lattice parameter of LAO (~3.790 Å)). The orientation relationship between the thin film and the substrate is as follows: $\pm[010]_{pc}$ of BFGO // $[001]_{pc}$ of the substrate (denoted as q_x) and the $\pm[\bar{1}01]_{pc}$ of BFGO // $[\bar{1}10]_{pc}$ of the substrate (denoted as q_y). It should be noted that the large *c*-axis (~ 4.6-4.7 Å) aligns only $\pm [\bar{1}10]_{pc}$ side. RSMs around 220 symmetric reflections of LAO along both the two in-plane directions are shown in Fig. 3-6a and b. The 202 peak positions of BFGO in these figures suggest that the $(101)_{pc}$ planes of GT phase tilt along only q_y side ($[\bar{1}10]_{pc}$)

from the substrate normal, as shown in insets of Fig. 3-6b. The anisotropic tilt only along the axis is presumably due to the large lattice mismatch between the *c* of GT phase (~ 4.6-4.7 Å) and the a_{pc} of LAO (~3.790 Å). The calculated tilt angle is ~ ±1.1° for the GT phase with smaller planes (labeled as GT1 in Fig3-6) and ~ ±0.74° for the GT phase with larger planes (labeled as GT2 in Fig3-6). Since the GT2 domain has a larger out-of-plane lattice spacing than GT1 phase, it is supposed to have a smaller in-plane lattice spacing than GT1 phase. Hence, the in-plane lattice mismatch against the substrate is expected to be smaller in GT2 phase than in GT1 phase. I believe that this is a reason of the tilt angles are different between the two domains. Figure 3-6c show a RSM around 221 asymmetric reflection of LAO. The *b*-axis length of BFGO is slightly relaxed from that of the LAO substrate along the q_x direction. It is also found that the q_z values of two BFGO peaks are smaller than those of 220 peaks, clearly indicating that BFGO has a monoclinic distortion with the polarization rotating toward $[010]_{pc}$ direction. Figure 3-6d shows a RSM around 120 asymmetric reflection of LAO. The q_y value of BFGO is considerably larger than that of LAO, indicating that BFGO thin films is completely relaxed along this direction presumably because of the large *c*-lattice parameter of BFGO. It is found that both the 201 and 021 peaks of BFGO are observed in Fig. 3-6d. Each peaks correspond to the domains where the *c*-axis of the GT phase points to $-q_y$ or $+q_y$ side, as shown in insets of Fig.3-6d. It can be seen that the 201 peak splits into two, which have different value of the lattice spacing. Therefore, I believe that the peak splitting results from the monoclinic distortion of a GT phase.

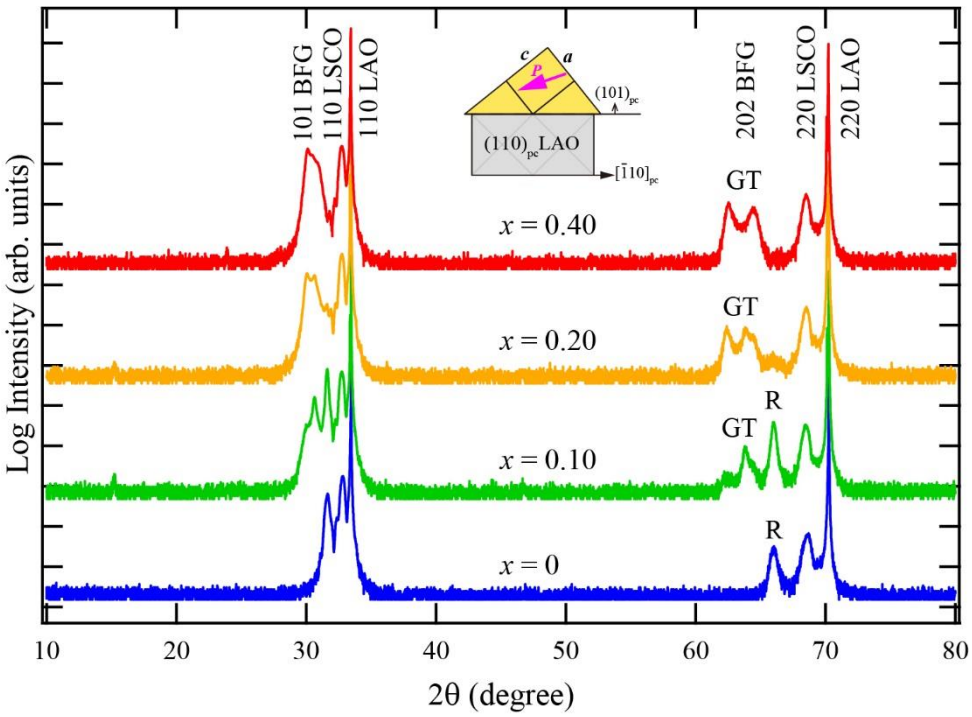

Figure 3-4. XRD θ–2θ patterns of BFGO thin films on $(110)_{pc}$-oriented LAO substrates. 'GT' and 'R' labels denote a giant *c*/*a* phase and a rhombohedral phase, respectively.

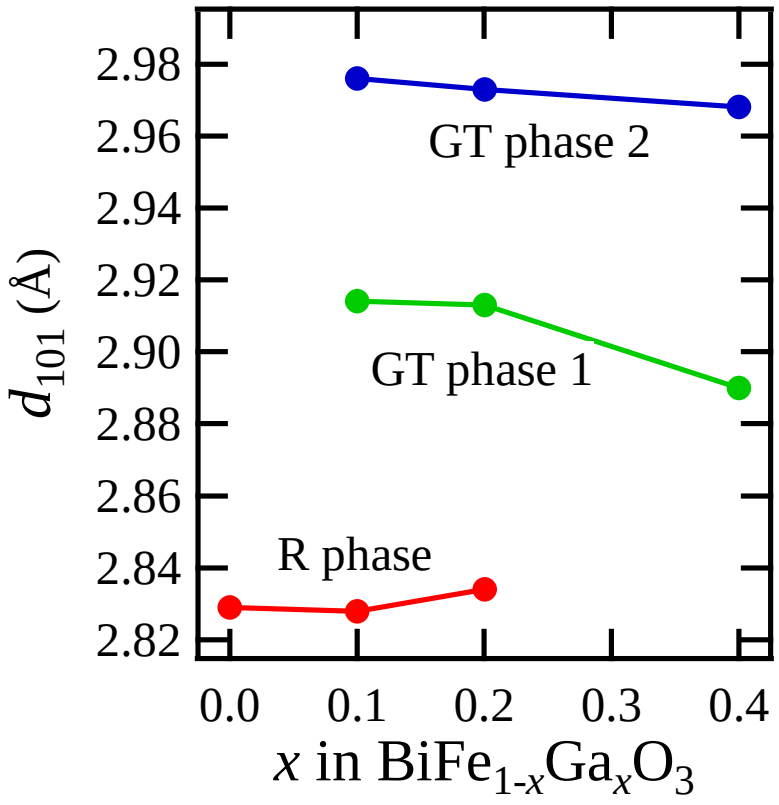

Figure 3-5. The out-of-plane *d* spacing of BFGO thin films on $(110)_{pc}$-oriented LAO substrates.

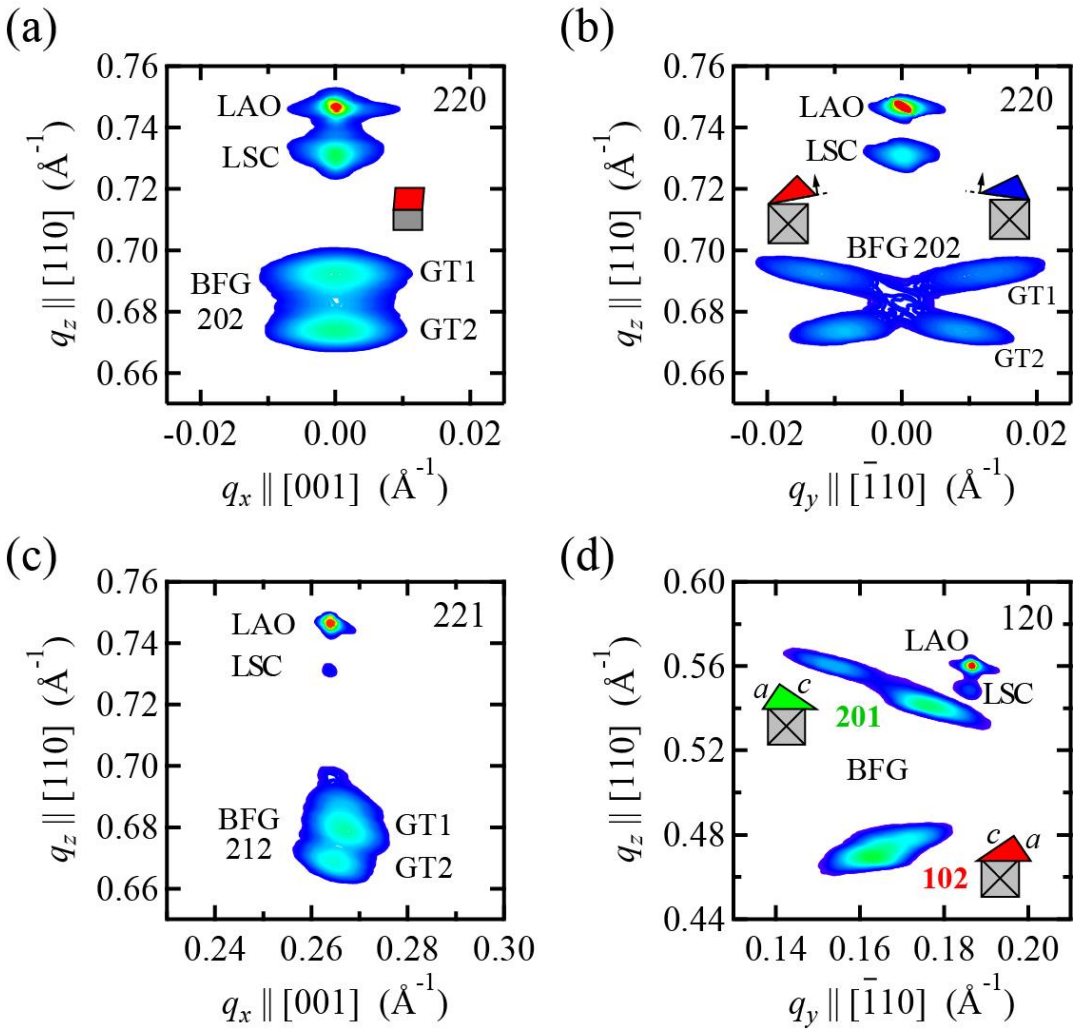

Figure 3-6. Reciprocal space mappings around 220, 221, and 120 LAO for BFGO thin films on $(001)_{pc}$-oriented LAO substrates with x = 0.10, 0.20, and 0.40.

3.3.2 Piezoelectric properties

3.3.2.1Thin films on $(001)_{pc}$–oriented $LaAlO_3$ substrates

Figure 3-7 shows the local piezoelectric strain versus electric field (*S*–*E*) curves for the $(001)_{pc}$–oriented BFGO thin films. It can be seen that the *S*–*E* curves have parallelogram-like shapes with large hysteresis. Since both phase transitions from M_C to M_A and from M_A to tetragonal in BFGO thin films are first-order as described above, it may also suggest the electric field induced phase transition occurred. Note that a similar behavior in *S*-*E* curve was reported in relaxor-ferroelectric PMN-PT, where a first order phase transition from a monoclinic to a tetragonal is induced by applying electric field. The effective piezoelectric constant S_{MAX}/E_{MAX} calculated from the *S*–*E* curves is plotted in Figure 3-8. The S_{MAX}/E_{MAX} value decreases from 39.8 to 36.8 pm/V as Ga content *x* increases in the M_C phase. This behavior is the same as that of the BFCO thin films, where the imposed epitaxial strain from the substrate becomes larger as Co content increases. The S_{MAX}/E_{MAX} values in the M_A structures are higher (48.5 for $x = 0.20$ and 49.6 pm/V for $x = 0.40$) than that in the M_C phases. This result is the same as that in BFCO thin films, indicating that a polarization rotation enhances a piezoelectric response even in monoclinic BFGO thin films and the polarization can rotate easier in the M_A phase than in the M_C phase. From Fig 3-7, the piezoelectric response seems to be enhanced by the electric field induced phase transition. A first order phase transition causes a drastic crystal structure change, leading to a discontinuous polarization rotation near the phase transition point. Therefore, it is considered that a discontinuous polarization rotation enhances the piezoelectric response in BFGO. The values of S_{max}/E_{max} of the BFGO thin films with the M_A phase are nearly comparable to those of BFCO thin films with the M_A phase. This is a natural consequence because the c/a ratio and the β angle of the BFGO thin films are nearly identical to those of the BFCO thin films.

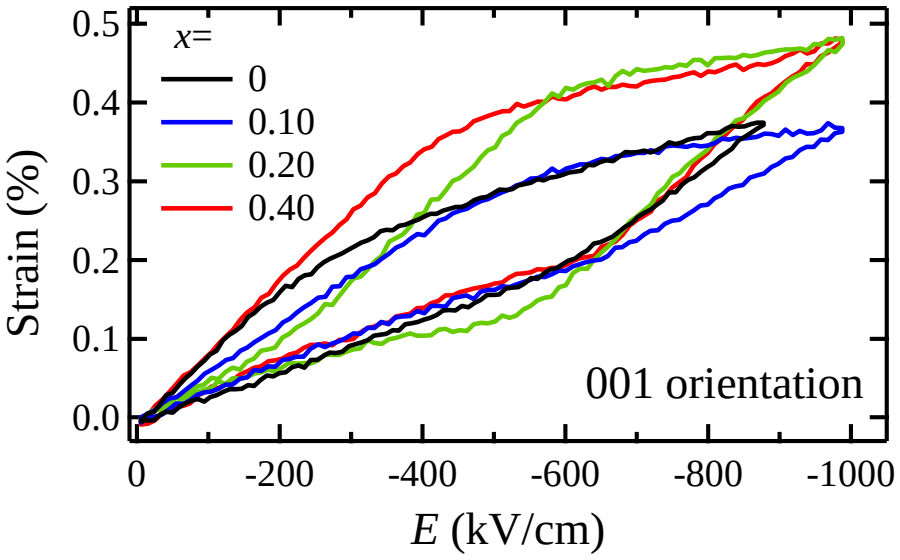

Figure 3-7. Local piezoelectric strain versus electric field curves for $(001)_{pc}$-oriented BFGO thin films.

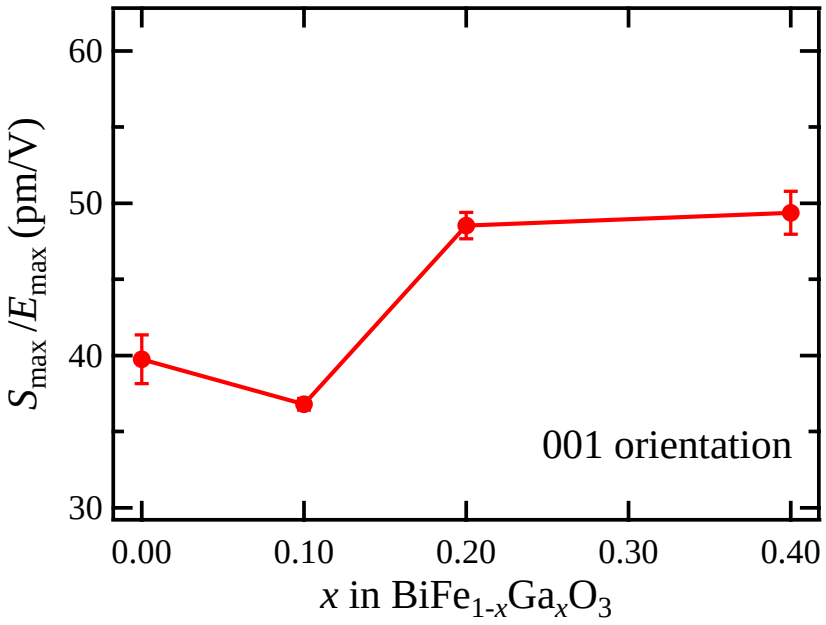

Figure 3-8. Effective piezoelectric constant S_{MAX}/E_{MAX} for $(001)_{pc}$-oriented BFGO thin films.

3.3.2.2 Thin films on $(110)_{pc}$–oriented $LaAlO_3$ substrates

Figure 3-9 shows local piezoelectric strain versus electric field (*S*–*E*) curves for $(101)_{pc}$-oriented BFGO thin films. The *S*–*E* curve of a pure BFO thin film with the rhombohedral phase (*x*=0) is almost linear without hysteresis. On the other hand, those of the BFGO with monoclinic GT phase (*x* = 0.10-0.40) have a large hysteresis. Such behavior is supposed to be due to a polarization rotation in the monoclinic phase. The effective piezoelectric constant S_{MAX}/E_{MAX} calculated from the *S*–*E* curves is plotted in Figure 3-10. The S_{MAX}/E_{MAX} value of the rhombohedral BFO (*x* = 0) is ~31.6 pm/V, comparable to that of a former report (~30 pm/V) on (101)-oriented BFO thin film on $SrTiO_3$ substrate [26]. It is clearly seen that the S_{MAX}/E_{MAX} value is drastically enhanced in the monoclinic GT phase and the value reaches ~80.1 pm/V at *x*= 0.40, which is 2.5 times as large as that in the rhombohedral BFO (*x*= 0). The S_{MAX}/E_{MAX} value of the films with GT phase increases from 65.8 to 80.1 pm/V as Ga content *x* increases from 0.10 to 0.40. This behavior can be explained by the decrease of the rhombohedral phase which has a smaller response than the monoclinic GT phase.

Next, the orientation dependence of the piezoelectric response is discussed. It is clearly seen that the S_{MAX}/E_{MAX} values of the monoclinic GT phase in the $(101)_{pc}$-orientation are superior to those in $(001)_{pc}$-orientation: The value at *x*=0.40 is 1.6 times as large as that in (001)-orientation. Such enhancement in the $(101)_{pc}$-orientation is not observed in a tetragonal perovskite with a large polarization such as $PbTiO_3$, where the maximum effective piezoelectric constant d_{33}^* is obtained along the polarization direction ([001]) and decreases monotonically as the tilting angle from polarization direction increases[79-81]. The enhancement of the piezoelectric response in the $(101)_{pc}$-orientation is a unique behavior in the monoclinic GT phase where polarization can rotate.

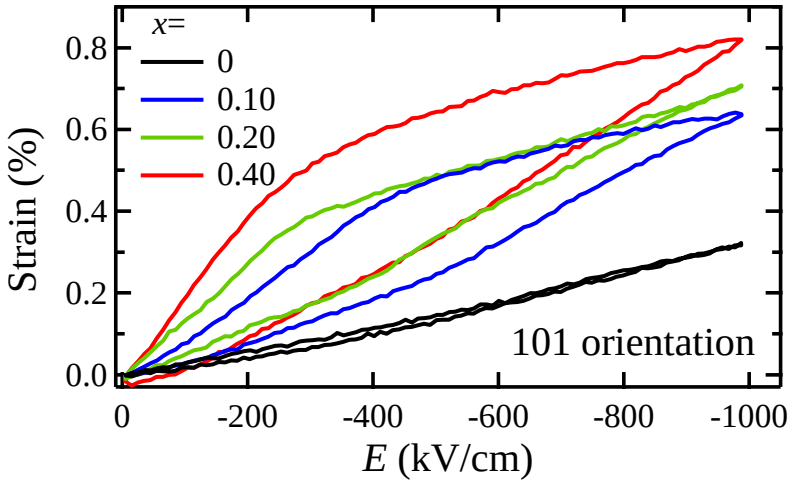

Figure 3-9. Local piezoelectric strain versus electric field curves for $(101)_{pc}$-oriented BFGO thin films on $(110)_{pc}$-oriented LAO substrates.

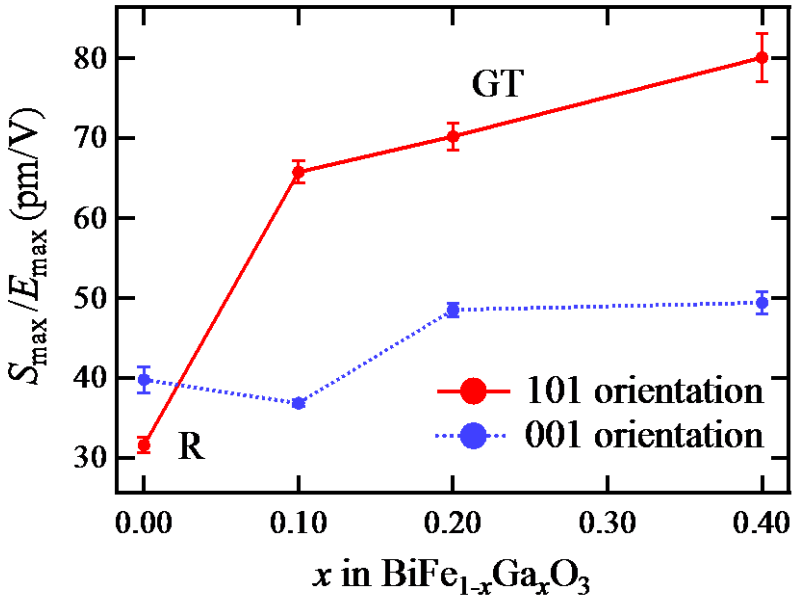

Figure 3-10. Effective piezoelectric constant S_{MAX}/E_{MAX} for $(101)_{pc}$-oriented BFGO thin films on $(110)_{pc}$-oriented LAO substrates.

3.4 Summary

In summary, the $BiFe_{1-x}Ga_xO_3$ (x = 0-0.40) thin films were prepared on $(001)_{pc}$ and $(110)_{pc}$-oriented (LAO) substrates and their piezoelectric properties were investigated. The M_A-type monoclinic BFGO with polarization rotation, which is the same as that of bulk powder samples and monoclinic $BiFe_{1-x}Co_xO_3$, was stabilized at x=0.20-0.40 in these orientations. The enhanced piezoelectric response due to polarization rotation was successfully confirmed in the $(001)_{pc}$-oriented monoclinic BFGO thin films. It was confirmed that all the BFGO thin films prepared on $(110)_{pc}$-oriented LAO substrates had a (101)-orientation and the structure changed from the rhombohedral (x = 0) to monoclinic phase with giant c/a ratio (x = 0.40) through two phase coexistence (x = 0.10, 0.20) as Ga content increases. The piezoelectric response of the $(101)_{pc}$-oriented monoclinic BFGO thin films with a giant c/a ratio is 1.6 times as large as that in $(001)_{pc}$-oriented one. Since such orientation dependent enhancement is not observed in an ordinal tetragonal phase with a large polarization, it is concluded that it is unique to the monoclinic phase where polarization can rotate.

Chapter 4

Direct observation of magnetization reversal by electric field at room temperature in $BiFe_{1-x}Co_xO_3$ thin film

4.1 Introduction

Electric field manipulation of magnetization is intensively investigated because of potential application in low-power-consumption non-volatile magnetic memory devises[43,82]. Despite the concentrated effort in the last 15 years on magnetic multilayers and magnetoelectric multiferroic thin films, no report was made on the reversal of out-of-plane magnetization by electric field at room temperature without the aid of electric current. In this chapter, I report the direct observation of out-of-plane magnetization reversal at room temperature by magnetic force microscope (MFM) after the electric polarization switching of Co substituted bismuth ferrite thin film grown on $(110)_o$-oriented $GdScO_3$(GSO) substrate. The striped pattern of the ferroelectric and weakly ferromagnetic domains was preserved after the reversals of out-of-plane electric polarization.

Currently, writing of magnetoresistive random access memory (MRAM) is achieved by the application of magnetic field generated by electric current or injection of spin current, both require current flow. Magnetization reversal by electric field is reported for a single component magnetoelectric multiferroic material, $Dy_{0.70}Tb_{0.30}FeO_3$, but at a low temperature of 1.85 K [51,83]. Bismuth ferrite, $BiFeO_3$ (BFO), is the most promising magnetoelectric multiferroic material due to its high antiferromagnetic Néel temperature (T_N) ~600 K, high ferroelectric Curie temperature (T_C) ~1100 K and the strong coupling between these two orders [1,7,8,53]. The crystal structure of BFO is a rhombohedral perovskite type with an *R*3*c* space group, where the electric polarization, mainly coming from Bi^{3+} ion displacement, is along $[111]_{pc}$ or $[001]_h$ direction (pc and h denotes pseudo-cubic or hexagonal notation, respectively) and FeO_6 octahedra have anti-phase rotation around the polar axis[84] ($a^-a^-a^-$ in Glazer's notation[85]). Generation of spontaneous magnetization by a spin canting due to spin-orbit interaction and breaking inversion symmetry induced by the FeO_6 octahedral rotation, known as Dzyaloshinskii-Moriya (DM) interaction, is theoretically predicted [56], but the presence of a long-ranged cycloidal modulation propagating along $<110>_h$ direction with a period of 62 nm [86]

prohibits the appearance of net magnetization. This cycloidal spin modulation disappears under strong magnetic field of over 18 T and a weak ferromagnetic moment of ~0.03 μ_B/f.u. is observed [53]. It has also been reported that the spin structure of BFO is quite sensitive to the epitaxial strain for thin film samples. BFO thin films grown on substrates with a large lattice mismatch such as $SrTiO_3$ (~ −1.7%) and $NdScO_3$ (~ 0.9%) had a collinear spin structure [55]. The free energy of the DM interaction is written as

$$E_{DM} = -\boldsymbol{D}\cdot(\boldsymbol{L}\times\boldsymbol{M}) \quad (1)$$

where $\boldsymbol{D}$ is DM vector, $\boldsymbol{L}$ is antiferromagnetic spin vector and $\boldsymbol{M}$ is weak ferromagnetism vector [56]. It should be noted that the DM vector in BFO is governed by the sense of rotation of the FeO_6 octahedra and aligned parallel or antiparallel along the electric polarization vector $\boldsymbol{P}$. Therefore, when antiferromagnetic spin vector lies in a plane perpendicular to polarization, a weak ferromagnetic moment is generated in the same plane, but the reliable report on the observation of such spontaneous magnetization in BFO film is absent.

Recently, J. T. Heron *et al.* predicted that polarization switching (including even 180° switching) can cause the change in octahedral rotations, hence the change in the DM vector[8]. Therefore, the weak magnetic moment is expected to be manipulated by polarization switching by applying electric field. They demonstrated an in-plane magnetization reversal of $Co_{0.9}Fe_{0.1}$ upper layer by a 180° polarization switching in BFO thin films by X-ray magnetic circular dichroism coupled to photoemission electron microscopy (XMCD-PEEM) imaging. However, the presence of CoFe upper layer complicates the interpretation of the experimental results including the way of coupling between the magnetic moment of CoFe alloy and that of BFO [87]. A single-phase material with ferroelectric and ferromagnetic orderings is crucial to study the intrinsic coupling between the two orders.

We have found that partial substitution of Co for Fe also stabilized the collinear phase with weak ferromagnetism preserving the *R*3*c* crystal structure up to $x = 0.20$ for $BiFe_{1-x}Co_xO_3$ [10]. Neutron powder diffraction and Mössbauer spectroscopy measurements on respectively $x = 0.2$ and 0.1 samples revealed the spin structure change from the cycloidal one at low temperatures to the collinear one at room temperature as schematically illustrated in Figs. 4-1a and 4-1b [54]. In the collinear phase the ordered spin moment lied in the $(001)_h$ plane, perpendicular to the electric polarization vector, indicating that the above discussed magnetic easy plane was not affected by Co substitution [10,54]. This result was consistent with our DFT calculation and the appearance of spontaneous magnetic moment of ~0.03 μ_B/f.u. in the $(001)_h$ plane was confirmed for thin film samples grown on (111)-oriented $SrTiO_3$ substrates [88]. It was

also indicated by the DFT calculation that the Co substitution increased the spin canting angle and enhanced the spontaneous magnetization [88]. The reorientation of the magnetic easy plane after ferroelectric poling was demonstrated through the remnant magnetization measurements on single crystals [11]. However, the in-plane nature of the magnetization of these thin film samples prohibited us from observing the magnetic domains by a local probe, *i.e*, MFM. The $(001)_{pc}$-oriented thin film is therefore favorable for the investigation of the magnetization reversal by electric polarization switching because the out-of-plane magnetization is expected to appear: the magnetic easy plane perpendicular to the polarization direction ($<111>_{pc}$) tilts from the film plane as illustrated in Fig. 4-1c.

Since the magnetic structure is quite sensitive to a lattice strain, the choice of single crystal substrate for thin film growth is of great importance [55,89]. Here, $(110)_o$-oriented $GdScO_3$(GSO) (a_{pc} ~3.969 Å) substrate was selected because of the small lattice mismatch (~0.5%). Indeed, BFO thin films grown on the GSO substrate had been reported to preserve the cycloidal spin structure, the same as that of bulk samples [55]. Our DFT calculation showed that the presence of Co substitution and 0.5% lattice mismatch do not affect the magnetic easy plane as shown in Fig. 4-1c.

4.2 Experiment

The BFCO (x= 0.10) thin films are prepared onto $(110)_o$-oriented $GdScO_3$ substrates using pulsed laser deposition technique with a KrF excimer laser (λ= 248 nm). A pulsed laser was focused on stoichiometric targets with an energy density of 1.5 J/cm^2. During the deposition, substrates temperature was kept at 690°C in an oxygen partial pressure of 15 Pa. Thicknesses of all thin films were fixed at 100 nm. $SrRuO_3$ (SRO) layer with a thickness of 30 nm was deposited as a bottom electrode.

The crystal structure of the thin films was investigated by X-ray diffraction with a Cu Kα radiation (XRD; Rigaku SmartLab).

^{57}Fe Mössbauer spectra was measured at room temperature for a nearly 100% ^{57}Fe-enriched BFCO thin films using conversion electron Mössbauer spectroscopy. ^{57}Co in an Rh matrix was used as a γ-ray source, and the Doppler velocity of the source was calibrated by using the standard spectrum of a α-Fe foil. The spectra were analyzed with standard software (Normos, made by R. A. Brand and commercially available from WissEl GmbH).

Temperature dependence of remanent magnetization of BFCO thin film was measured using a superconducting quantum interference device (SQUID) magnetometer. After a magnetic poling of 5 T at room temperature, a remnant magnetization (M_r) was

measured at 0 T on cooling from 400 K to 5 K. To reduce the contribution of the GSO substrate, the thickness was reduced from ~500 μm to ~40 μm by polishing a substrate (like TEM sample preparation). Note that a non-magnetic sapphire substrate was glued to the sample by epoxy adhesive as reinforcing material.

PFM and MFM observation were performed using a scanning probe microscope (Cypher, Asylum Research). PFM is one of the scan modes of AFM to analyze a ferroelectric domain structure of a sample. When the sample has piezoelectricity, a piezoelectric strain is induced by an application of an AC bias. A conductive cantilever is directly contacted on the sample surface to be used as an upper electrode in a capacitor structure. In PFM, the piezoelectric response of the sample is detected as a cantilever deflection signal. The vertical and lateral PFM images were obtained using dual ac resonance tracking PFM (DART-PFM). An ac voltage of 3 V at a frequency of ~ 250 KHz (vertical) or ~ 900 KHz (lateral) was applied to a conductive cantilever (ASYELEC-01) to obtain PFM contrast. An in-plane PFM scan performed along $<110>_{pc}$ direction can discriminate only 2 of 4 variants, corresponding that in-plane polarization direction is left or right side of a cantilever. Hence, two in-plane PFM, where in-plane scanning angle is 0° and 90° against $[110]_{pc}$ direction, and one out-of-plane PFM measurements were performed to obtain a total PFM image. The total PFM image was created by merging the three obtained images, using commercial photo-editing software. MFM images were obtained using a hard magnetic coated cantilever (MFMR, Nanoworld). MFM is one of the scan modes of AFM to analyze the magnetic domain structure of the sample. The stray field from the sample surface is detected by a ferromagnetic material coated cantilever. The lift height in MFM measurement is set to 20 nm. To distinguish magnetic force from other force such as electrostatic one, we performed two MFM scans in which a magnetization direction on tip poled upward and downward.

4.3 Results and discussion

4.3.1 Crystal structure

Figure 4-1d shows the θ-2θ XRD pattern of $BiFe_{0.9}Co_{0.1}O_3$ (BFCO) thin film grown on $(110)_o$-oriented GSO substrate. It is confirmed that the highly crystalline BFCO thin film is $(001)_{pc}$-oriented and without detectable impurity phases. Figure 4-1e shows reciprocal space mappings (RSM) around $510_o(203_{pc})$ and $442_o(113_{pc})$ reflections of GSO. The 203_{pc} and the 113_{pc} reflections of BFCO split into two and three spots, respectively, indicating that the crystal structure is a rhombohedral-like monoclinic one, the same as that of BFO thin films on the GSO substrates[62]. The lattice parameters a_m, b_m, c_m, and β are 5.637($\sqrt{2}\times3.986$) Å, 5.594($\sqrt{2}\times3.955$) Å, 3.941 Å, and 89.33°, respectively. Note that the monoclinic unit cell is defined as $\sqrt{2}\ a_{pc} \times \sqrt{2}\ b_{pc} \times c_{pc}$ [62,90,91], as shown in the inset of Fig. 4-1d. The out-of-plane lattice parameter c_m is slightly smaller than an average of the in-plane lattice parameters ($(a_m+b_m)/2\sqrt{2} \sim 3.971$ Å), indicating that a moderate tensile strain (~0.47%) is imposed on the BFCO thin film. Therefore the BFCO thin films are expected to preserve the same collinear spin structure as that of bulk samples.

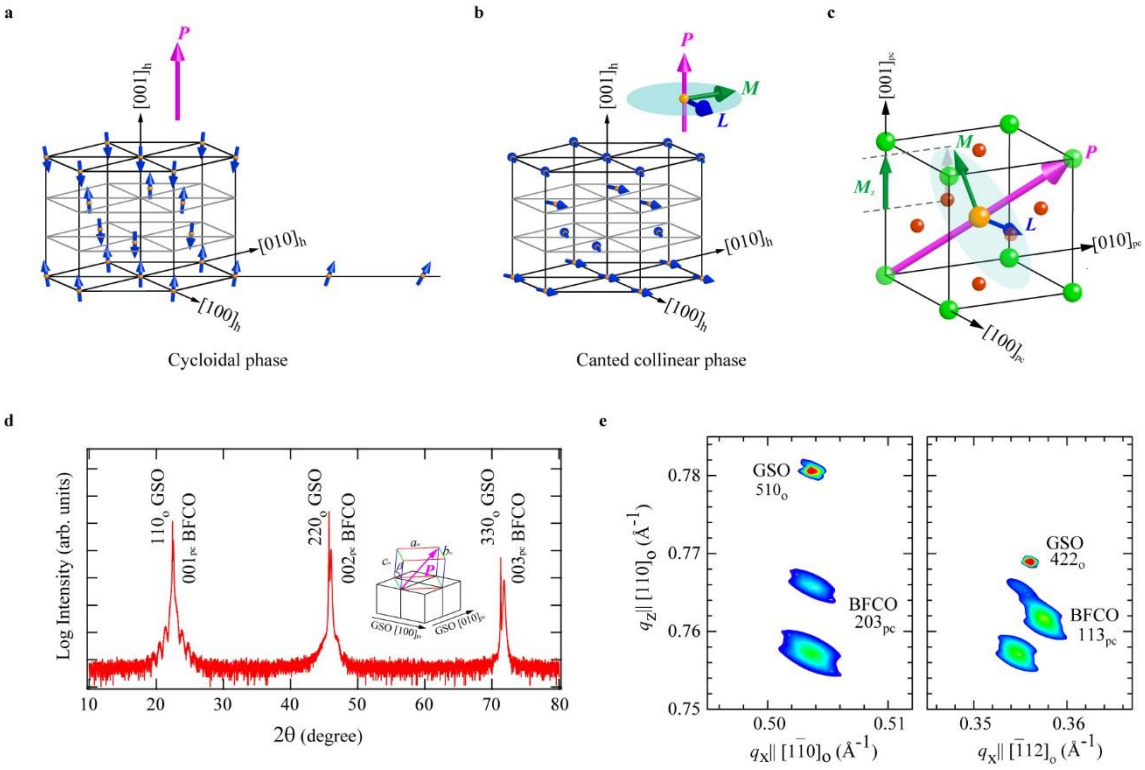

Figure 4-1 Magnetic structure of multiferroic BFCO, presence of out-of-plane magnetization in $(001)_{pc}$-orientated BFCO thin film and confirmation of the orientation. **a**, The cycloidal phase with a modulation propagating along $<110>_h$ direction without a net magnetization, which is stable below 200 K for x=0.1 BFCO. **b**, The canted collinear phase with a weak ferromagnetic moment ***M*** (green arrow), which is stable at room temperature for x=0.1 BFCO. The weak ferromagnetic moment lies in a plane perpendicular to the polarization vector, ***P*** (pink arrow). Orange spheres represent magnetic Fe/Co ions and small blue arrows represent the spins at Fe/Co sites. **c,** Schematics of out-of-plane magnetization in $(001)_{pc}$-oriented BFCO thin film. Since a magnetic easy plane (blue disk) is perpendicular to polarization vector ***P***, the out-of-plane magnetization $\boldsymbol{M}_z$ can appear. **d**, The XRD diffraction θ-2θ profile of the BFCO thin film. Only 00l peaks of BFCO are observed except for the peaks of the GSO substrate. The inset is a monoclinic unit cell of BFCO defined as $\sqrt{2}\ a_{pc} \times \sqrt{2}\ b_{pc} \times c_{pc}$ **e**, Reciprocal space maps of the BFCO thin film around 510_o and 422_o GSO substrate.

4.3.2 Magnetic properties

The collinear spin structure of the BFCO thin film on GSO substrate was confirmed by conversion electron Mössbauer spectroscopy (CEMS) on a ~100% ^{57}Fe-enriched thin film sample. The bottom of Figure 4-2a shows the CEMS spectrum of the BFCO thin film at room temperature. The spectrum is symmetric in the height and the width, whereas the spectrum of the BFO thin film on the same substrate with a cycloidal spin structure (the top of Fig. 2a) is asymmetric [55]. The data for BFCO film is well fitted with one magnetic component, which has a Zeeman sextet with a symmetric height and an isomer shift (IS) of 0.385 mm/s, quadrupole shift (QS) of −0.217 mm/s, and hyperfine field (B_{hf}) of 47.7 T, indicating that the magnetic structure is the collinear one. The value of IS is characteristic of Fe^{3+} ions in octahedral coordination. The value of QS is close to that of bulk BFCO (-0.20 mm/s) and that of (111)-oriented BFCO thin films (-0.217 mm/s)[20,21], strongly suggesting that the spins are aligned perpendicular to the electric field gradient (V_{zz} >0[54]) which is along the polar axis. This indicates that the BFCO thin film on GSO substrate has a magnetic easy plane perpendicular to the electric polarization axis (Fig. 4-2b) as in the case of bulk and (111)-oriented thin film samples[54,88]. The area intensity ratio of six lines is 3:2.62:1:1:2.62:3, indicating that the angle between the ordered spin moment (antiferromagnetic spin vector) and the incident direction of γ-ray, the substrate normal direction in this case, is ~63° (Fig. 4-2c). Taking into account another condition, $\boldsymbol{L} \perp \boldsymbol{P}$ ($[11\bar{1}]_{pc}$ direction), the possible directions of $\boldsymbol{L}$ are limited to be four as schematically illustrated in Fig. 4-2d. These are quite close to $[\bar{1}21]_{pc}$, $[2\bar{1}1]_{pc}$, $[1\bar{2}\bar{1}]_{pc}$ and $[\bar{2}1\bar{1}]_{pc}$. Since $\boldsymbol{L}$ are in four of six <$\bar{1}$21> directions in the easy plane perpendicular to $\boldsymbol{P}$ along $[11\bar{1}]$ direction (blue colored directions in Fig. 4-2e), it is reasonable to assume that BFCO has six magnetic favorable spin directions and two of these were not chosen most probably because of the epitaxial strain. The presence of magnetic easy axis was predicted for highly strained BFO film [92]. Each ferroelectric domain has four possible magnetization directions, all of which have the out-of-plane ferromagnetic component. Spontaneous magnetization $\boldsymbol{M}$ is in four <110> directions, perpendicular to both $\boldsymbol{L}$ and $\boldsymbol{P}$. Magnetization reversal by 71° ferroelectric switching is expected if the octahedral rotation is accompanied by the change in the $\boldsymbol{L}$ direction (Fig. 4-2f). The presence of spontaneous magnetization was confirmed by remnant magnetization measurement using a superconducting quantum interference device (SQUID) magnetometer. As shown in Fig. 4-3a and b, by reducing the thickness of a GSO substrate which has a large paramagnetic contribution from Gd^{3+} down to ~40 μm, the decrease in the out-of-plane magnetization of the BFCO thin films at low temperature owing to the spin structure change to the nonmagnetic cycloidal one was successfully observed.

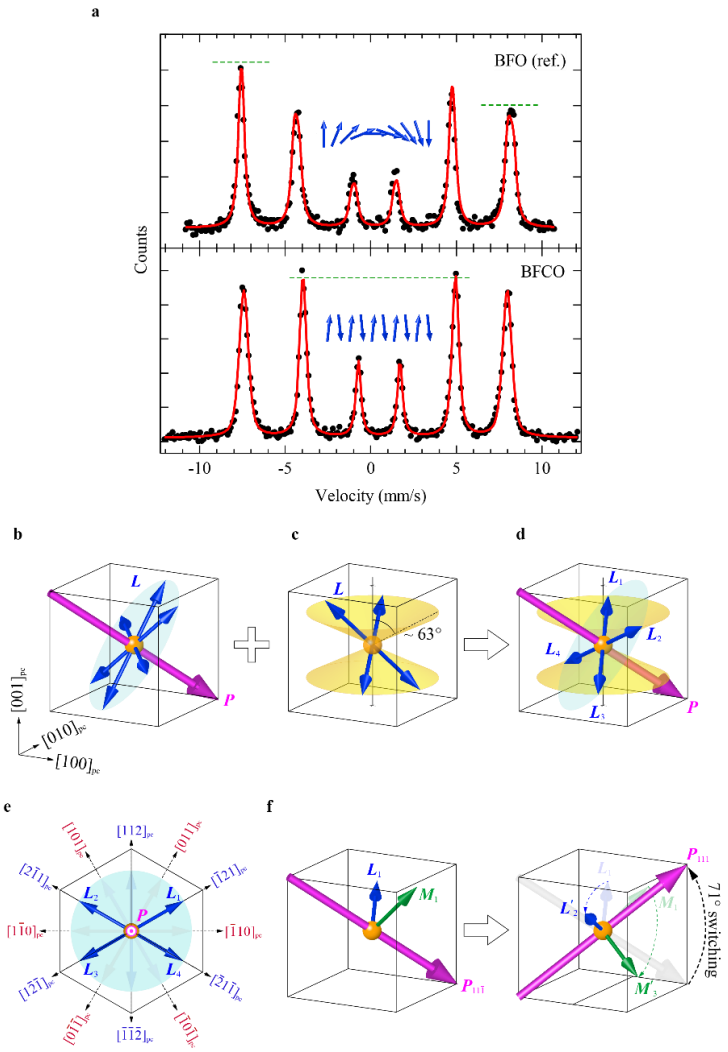

Figure 4-2 Spin structure of BFCO thin film**. a**, The CEMS spectrum for BFO thin film on GSO substrate (top) reported by D. Sando *et al*. [55] (Copyright 2013, Nature publishing Group) and the BFCO thin film on GSO substrate (bottom). The insets are the schematics of a cycloidal phase and a canted collinear phase, respectively. **b**, The spin direction ***L*** determined from a QS value. The spin is on a magnetic easy plane (blue disk) perpendicular to polarization vector ***P***. **c**, The spin tilt angle of ~ 63° from a film normal determined by the area intensity ratio of the CEMS spectra. The spin is on two yellow cones, the apex angle of which is ~ 2×63°. **d**, The possible spin structure of the BFCO thin film satisfying both the conditions of 3b and 3c. Assuming that a polarization points to [11$\bar{1}$] direction, the 4 magnetic states are allowed. All of them possess the out-of-plane magnetic moment. **e**, The configuration of ***L*** vectors in the easy plane viewed from ***P*** direction. These align along 4 of 6 <$\bar{1}$21> directions. **f**, One of the possible magnetization switching process accompanied with a out-of-plane 71° polarization switching, where the out-of-plane magnetization is reversed.

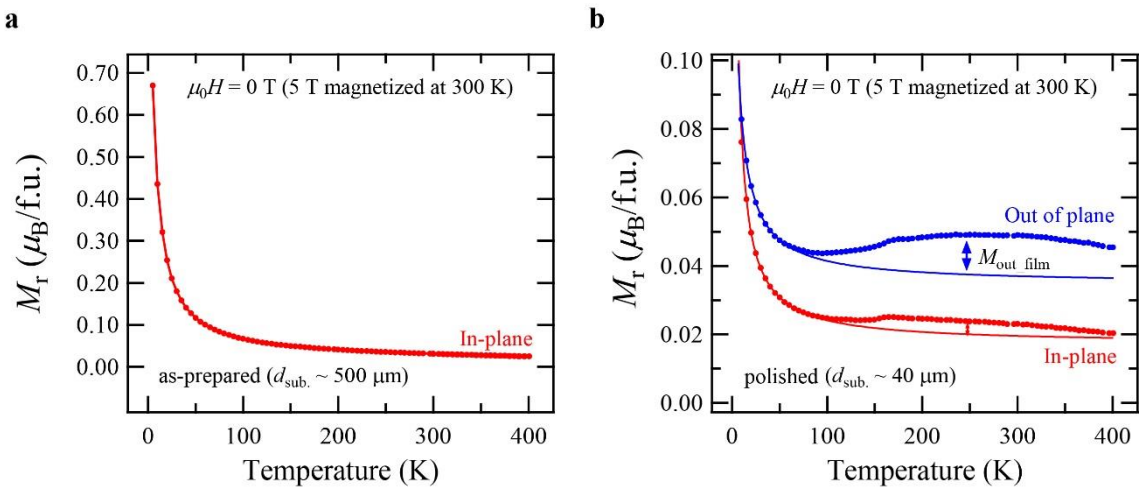

Figure 4-3 |Temperature dependence of remanent magnetization (M_r) of a BFCO thin film on GSO substrate. **a** as-prepared sample. **b** polished sample. The $d_{sub.}$ denotes the thickness of the GSO substrate. The red and blue solid lines in Fig. 4-3a and b are the paramagnetic component of the substrate extracted by Curie-Weiss fitting below the transition.

4.3.3 Demonstration of a magnetization reversal by polarization switching

The correlation between ferroelectric and ferromagnetic domains was investigated by piezoelectric force microscopy (PFM) and MFM observations on the as-grown BFCO thin film. Since the polarization directions in the monoclinic phase are close to $<111>_{pc}$, there are eight possible ferroelectric domains variant with four polarization upward and four polarization downward against the film normal, as shown in Fig 4-4a. Figure 4-4c shows the total PFM image of 6 μm × 6 μm area. A striped domain configuration with four polarization down domains was observed. All of the adjacent domains have 71° domain walls. It is well known that such striped domain structure commonly appears in BFO and other ferroelectric thin films in order to minimize the electrostatic and elastic energies [93-96].

Figure 4-4d shows a MFM phase image of the same area. The ferromagnetic domains form striped structure similar to that of the ferroelectric domain, indicating that both domains are strongly coupled with each other. It should be noted that a reversal of magnetization of the cantilever causes a reversal of the MFM image contrast, unambiguously confirming that the contrast comes from magnetic interaction, not from the electrostatic one. These results are consistent with the X-ray magnetic linear dichroism coupled to photoemission electron microscopy (XMLD-PEEM) observation of a BFO thin film by T. Zhao *et al.*[7] where the antiferromagnetic domains are coupled with the ferroelectric domains.

Finally, the magnetization reversal by a polarization switching was demonstrated. A poling scan with $[1\bar{1}0]_{pc}$ slow scan direction and a -7 V tip bias was conducted on a box region of 4 μm × 4 μm area, as shown in Fig. 4-4b. A total PFM image after a poling scan is shown in Fig. 4-4e. The out-of-plane polarization component is successfully switched from downward to upward in the entire poled region. It is remarkable that there are only three domains colored with red, pink, and yellow and no orange domain with $[1\bar{1}0]_{pc}$ in-plane polarization is observed with the exception of boundary regions. This is because of an effective in-plane electric field created by a cantilever motion during the poling scan, a so-called trailing field [95-97]. In the case of a box poling scan (like Fig. 4-4b), the in-plane field is only activated along the slow scan axis because trace and retrace scans cancel out the field during each fast scan [95]. In the present poling scan, the induced trailing field points to the $[1\bar{1}0]_{pc}$ direction, therefore the orange domain with $[\bar{1}10]_{pc}$ in-plane polarization is electrostatically unfavorable and can no longer exist .

Figure 4-4f shows the MFM phase image after the poling. It is clearly seen that the out-of-plane magnetization is changed drastically by the poling and the magnetic domain structure is coupled with the ferroelectric domain structure after the poling but not the

one before the poling. This is the first direct observation of a magnetization switching in BFO-based single phase thin films by polarization switching. It seems that the phase contrast in left and right side near the poling region gets a phase shift (i.e. becomes red color in this image). This is presumably due to an influence of an electrostatic force in the poled region[98]. It does not mean that the magnetization in this region changed by the poling.

Figures 4-5a-d, and 4-5e-h are the magnified views of areas (i) and (ii) in Fig. 4-4c. Almost identical striped domain structure is observed after the poling in area (i) with in-plane polarization direction unchanged as shown in figs. 4-5a and 4-5c, indicating that pure out-of-plane 71° domain switching occurred in this area. On the other hand, the striped domain structure is drastically modified in area (ii). The in-plane polarization direction is also changed in addition to the out-of-plane switching, as shown in Figs. 4-5e and g. Such a different behavior between two regions is attributed to the difference in the in-plane polarization directions in the initial domain structures. The net in-plane polarization (P_{ip_net}), vector sum of the in-plane electric polarization of each domain, in area (i) points to the lower right direction. It therefore conforms to the $[1\bar{1}0]_{pc}$ trailing field. On the other hand, P_{ip_net} in area (ii) is pointing to upper right direction and is changed to the lower right direction by the trailing field. The magnetic domain structure in area (i) is also preserved, as shown by MFM phase contrast in Figs 4-5b and 4.5d, but the color is reversed, indicating that the out-of-plane magnetization is switched from downward to upward and *vice vasa* in this area. This is the first direct observation of magnetization reversal by electric field at room temperature. On the other hand, although the MFM phase contrast certainly changed by the poling in area (ii), the contrast is correlated with the ferroelectric domain structure after the poling as shown in Figs. 4-5f and 4-5g. These results deterministically indicate that an out-of-plane magnetization reversal can be achieved by 71° polarization switching without the ferroelectric domain reconstruction. It must be mentioned that for clarity, I intentionally shifted the positions in Fig. 4-5a-h because the position of magnetic domain and ferroelectric domain is not completely matched. I believe that this is due to a difference of the surface sensitivity between MFM and PFM methods and inclination of 71°ferroelectric domain wall against film normal. Note that J. T. Heron *et al*. reported that an in-plane magnetization of $Co_{0.9}Fe_{0.1}$ upper layer was reversed by 180° polarization switching in BFO thin films[8]. Therefore, the most important point to achieve magnetization reversal by polarization switching may be preserving ferroelectric domain structure during a poling, and hence 71° switching is not a prerequisite.

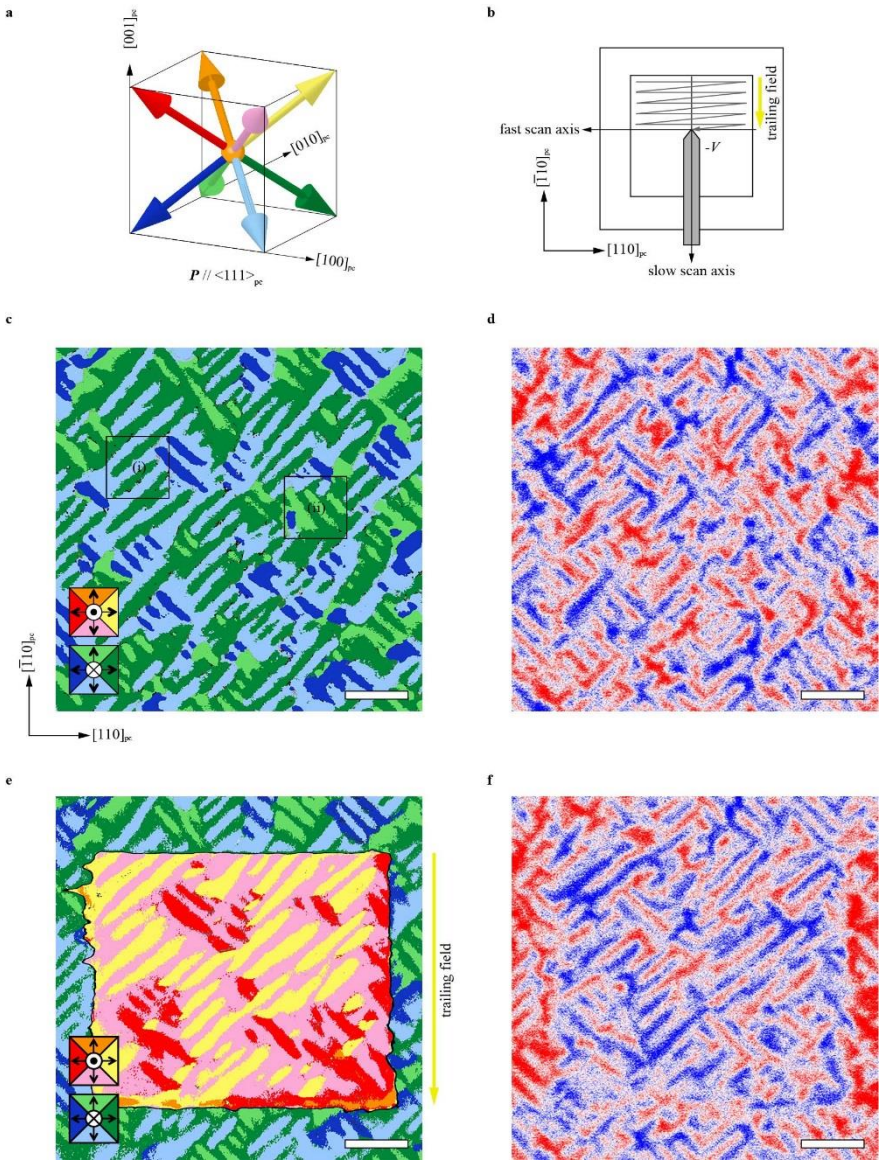

Figure 4-4 |The correlation between ferroelectric and ferromagnetic domains in the BFCO thin film. **a**, Possible polarization directions of the BFCO thin film. The framework indicates pseudo-cubic cell. Each arrow indicates polarization vector along <111> directions **b**, The configuration of the poling scan. The trailing field along slow scan direction $[1\bar{1}0]_{pc}$ is generated by a cantilever motion. **c-d**, Total PFM (c) and MFM phase (d) images for as-grown BFCO thin film. The color of each domain in PFM image corresponds the polarization direction. The relationship is shown in the left bottom indicator. The color in MFM image corresponds to out-of-plane magnetization direction. **e-f**, Total PFM (e) and MFM phase (f) images after a poling for BFCO thin film. Yellow arrow indicates the trailing field generated by a poling scan. The white scale bar in Fig.3 e-f corresponds to 1 μm.

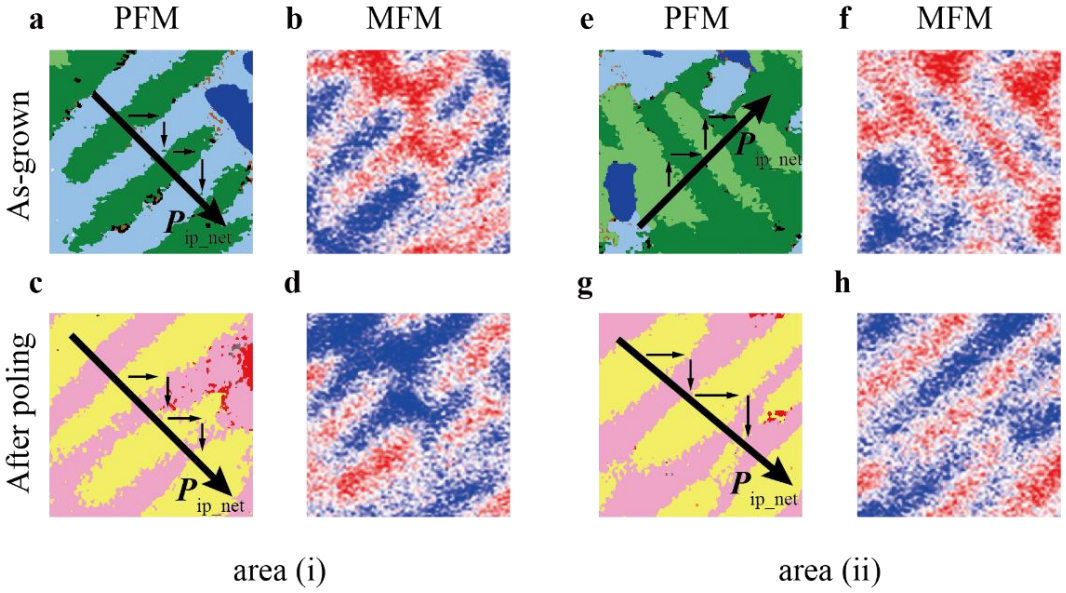

Figure 4-5 | Magnetization reversal by a polarization switching for BFCO thin films. **a-d**, Total PFM (a,c) and MFM phase (b,d) images for as-grown (a,b) and after a poling(c,d) BFCO thin film at area (i) in Fig. 3c. e-h, Total PFM (e,f) and MFM phase (g,h) images for as-grown and after a poling BFCO thin film at area (ii) in Fig. 3c. An out-of-plane magnetization switching can be achieved by 71° polarization switching without the ferroelectric domain reconstruction. The area in these images is 1 μm×1 μm.

4.4 Summary

Finally, I evaluate the possibility of integration necessary for memory device application. The complicated stripe domain structure in BFCO makes it difficult to perform reliable magnetization reversal by polarization switching at a fixed position. Controlled patterning of the single ferroelectric domain structure is necessary. It will be achieved by making island structure by using patterned musk during the film growth or lithography after the film fabrication [99]. Then the ferroelectric switching will be performed with the top electrode. The magnetization reversal will be detected by the Hall device prepared on the electrode. I estimate the magnetic field generated by BFCO to be 0.6 mT when the thickness of the electrode is 50 nm, which is well above the detection limit of InSb Hall sensor. Thus, I conclude that BFCO sufficiently satisfies prerequisites for memory device application.

In summary, I have confirmed that a single-phase ferromagnetic ferroelectric BFCO thin film grown on $(110)_o$-oriented GSO substrate had a canted collinear spin structure with an out-of-plane magnetization by Mössbauer spectroscopy. Moreover, I have observed an out-of-plane magnetization reversal by a 71° polarization switching without ferroelectric domain reconstruction by magnetic force microscopy and piezoelectric force microscopy. The current demonstration of a magnetic reversal by electric field paves the avenue to the integrated low-power-consumption MRAM.

Chapter 5 Conclusion and future perspectives

5.1 Conclusion

In this thesis, piezoelectric and multiferroic properties of $BiFeO_3$-based thin films are studied. As mentioned in the chapter 1, the objective in this thesis is to reveal a capability of Bi-containing perovskite oxide as advanced functional electric materials.

The results are summarized as follows:

In the chapter 2, the monoclinic $BiFe_{1-x}Co_xO_3$ (x = 0-0.50) epitaxial thin films with a giant c/a ratio were prepared and their piezoelectric response was evaluated. Three different phases were successfully obtained: a M_C-type monoclinic (x = 0–0.15), a M_A-type monoclinic (x = 0.15–0.30), and a tetragonal (x = 0.50). The M_A phase is essentially the same as that found in bulk BFCO where polarization rotation has been found. The enhanced piezoelectric responses were shown in the M_A and M_C type monoclinic phases, especially in the M_A phase, unambiguously indicating that this is due to polarization rotation in monoclinic phase. A larger deviation in the β angle from 90° in the M_A phase leads to enhanced piezoelectric response, which can be attributed to more room for polarization to rotate.

In the chapter 3, the $BiFe_{1-x}Ga_xO_3$ (x = 0-0.40) thin films were prepared on $(001)_{pc}$ and $(110)_{pc}$-oriented (LAO) substrates and their piezoelectric properties were investigated. The enhanced piezoelectric response due to polarization rotation was successfully observed in the $(001)_{pc}$-oriented M_A phase BFGO thin films. It was confirmed that all the BFGO thin films prepared on $(110)_{pc}$-oriented LAO substrates had a (101)-orientation and the structure changed from the rhombohedral (x = 0) to monoclinic phase with giant c/a ratio (x = 0.40) through two phase coexistence (x = 0.10, 0.20) as Ga content increases. The piezoelectric response of the $(101)_{pc}$-oriented monoclinic BFGO thin films with a giant c/a ratio is 1.6 times as large as that in $(001)_{pc}$-oriented one. Since such enhancement cannot be observed in an ordinal tetragonal phase with a large polarization, it is concluded that it is unique to a monoclinic phase where polarization can rotate.

In the chapter 4, a single-phase ferromagnetic ferroelectric BFCO thin film was prepared on $(110)_o$-oriented GSO substrate and a magnetization switching mechanism of $BiFeO_3$-based multiferroic materials was elucidated through a direct observation of magnetization reversal by electric field. The thin film with a moderate tensile strain had an out-of-plane magnetization confirmed by Mössbauer spectroscopy and SQUID

magnetometry. It was elucidated that the magnetization was able to be controlled by applying electric field and the 71° polarization switching without ferroelectric domain reconstruction was crucial to reverse the out-of-plane magnetization.

From the results in the chapter 2 and 3, it is proposed that a realization of the M_A-type monoclinic phase with polarization rotation is a promising concept for development of a novel Bi-containing piezoelectric perovskite: Furthermore, an orientation control of the monoclinic thin film with polarization rotation has a great potential to enhance the response in the Bi-containing piezoelectric perovskite. Therefore, it is suggested that Bi-containing piezoelectric perovskites still have a room for an improvement of the piezoelectric response.

As mentioned in the chapter 1, $BiFe_{1-x}Co_xO_3$ has three distinct structure phases: rhombohedral, monoclinic and tetragonal. In the chapter 2 and 4, I succeeded in preparing all the three phases and revealed that the monoclinic phase was a remarkable piezoelectric material with polarization rotation and the rhombohedral phase was a room-temperature multiferroic material where the magnetization can be controlled by polarization switching. From these results, it is concluded that BFCO is a promising material as piezoelectric and multiferroic material.

The conclusion of above results is that Bi-containing piezoelectric perovskite has a great capability for the piezoelectric and room temperature magnetoelectric applications.

5.2 Future perspectives

5.2.1 Realization of high piezoelectric response in Bi-containing piezoelectric materials

Although an enhancement of the piezoelectric responses due to polarization rotation were observed in the monoclinic Co and Ga-substituted $BiFeO_3$ with a giant *c*/*a* ratio, the responses are still lower than that of PZT. This is presumably due to the large polarization in this phase. The realization of a M_A–type monoclinic phase with a smaller spontaneous polarization is promising to achieve a high piezoelectric response. A M_A-type monoclinic phase with a *Cm* space group has found in $BiGa_{1-x}M_xO_3$ (M= Al, Cr, Mn) [3,39]. Therefore, the enhanced piezoelectric response due to polarization rotation is also expected in these materials. Among them, $BiGa_{0.25}Al_{0.75}O_3$ is expected to be a promising piezoelectric material because of the high resistivity due to the d^0 and d^{10} electronic configuration of Al^{3+} and Ga^{3+} in this material.

It was confirmed that the $(101)_{pc}$-oriented monoclinic BFGO thin films with a giant *c*/*a* ratio had a larger piezoelectric response than the $(001)_{pc}$-oriented one. Since the lattice

parameters *a* and *b* are more sensitive to polarization rotation than the *c*-lattice parameter in the monoclinic BFCO, Further enhancement of piezoelectric response could be expected in $(110)_{pc}$-orientated one. Unfortunately, there are no suitable perovskite substrate where such epitaxial growth can be acceptable. Therefore it is necessary to introduce a buffer layer or to attempt heteroepitaxial growth on non-perovskite substrate.

5.2.2 $BiFeO_3$-based multiferroic materials for the multiferroic memory applications.

Complicated stripe domain structure in Co-substituted $BiFeO_3$ thin film makes it difficult for application of memory devices: Thin film with a single stripe structure or a pure single domain structure is desired. Such domain structure can be achieved in BFO thin film on $(110)_O$-oriented $DyScO_3$ substrate prepared under optimal condition or on miscut (001)-oriented $SrTiO_3$ substrate[94,95], it would be also achievable in BFCO thin film.

Since the ferromagnetic ferroelectric Co-substituted $BiFeO_3$ thin film has a low resistivity and a high coercive field, I have never succeeded in repetitive magnetization reversal by polarization switching by PFM. It is suggested that third element substitution for Fe/Co site is promising to improve the resistivity and reduce the coercive field. It has been reported that La-substitution for Bi in $BiFeO_3$ greatly reduce the coercive field. This implement could also be effective in Co-substituted $BiFeO_3$ [100].

Reference

[1] G. Catalan and J. F. Scott, Advanced Materials **21**, 2463 (2009).

[2] M. R. Suchomel, A. M. Fogg, M. Allix, H. J. Niu, J. B. Claridge, and M. J. Rosseinsky, Chemistry of Materials **18**, 4987 (2006).

[3] A. A. Belik, T. Wuernisha, T. Kamiyama, K. Mori, M. Maie, T. Nagai, Y. Matsui, and E. Takayama-Muromachi, Chemistry of Materials **18**, 133 (2006).

[4] T. Kimura, S. Kawamoto, I. Yamada, M. Azuma, M. Takano, and Y. Tokura, Physical Review B **67**, 180401 (2003).

[5] A. A. Belik *et al.*, Chemistry of Materials **18**, 798 (2006).

[6] J. Wang *et al.*, Science **299**, 1719 (2003).

[7] T. Zhao *et al.*, Nature Materials **5**, 823 (2006).

[8] J. T. Heron *et al.*, Nature **516**, 370 (2014).

[9] C. Ederer and N. A. Spaldin, Physical Review Letters **95**, 257601 (2005).

[10] I. Sosnowska, M. Azuma, R. Przenioslo, D. Wardecki, W. T. Chen, K. Oka, and Y. Shimakawa, Inorganic Chemistry **52**, 13269 (2013).

[11] H. Yamamoto, Y. Sakai, K. Shigematsu, T. Aoyama, T. Kimura, and M. Azuma, Inorganic Chemistry **56**, 151717 (2017).

[12] G. Shirane, K. Suzuki, and A. Takeda, J. Appl. Phys. **25**, 809 (1954).

[13] B. Jaffe, W. R. Cook, and H. Jaffe, Piezoelectic Ceramics (Academic Press, London, 1971).

[14] B. Jaffe, R. S. Roth, and S. Marzullo, J. Appl. Phys. **25**, 809 (1954).

[15] B. Noheda, D. E. Cox, G. Shirane, J. A. Gonzalo, L. E. Cross, and S. E. Park, Applied Physics Letters **74**, 2059 (1999).

[16] H. X. Fu and R. E. Cohen, Nature **403**, 281 (2000).

[17] L. Bellaiche, A. Garcia, and D. Vanderbilt, Physical Review Letters **84**, 5427 (2000).

[18] L. Bellaiche, A. Garcia, and D. Vanderbilt, Physical Review B **64**, 060103 (2001).

[19] D. Vanderbilt and M. H. Cohen, Physical Review B **63**, 9, 094108 (2001).

[20] R. E. Cohen, Nature **358**, 136 (1992).

[21] Y. Kuroiwa, S. Aoyagi, A. Sawada, J. Harada, E. Nishibori, M. Takata, and M. Sakata, Physical Review Letters **87**, 217601 (2001).

[22] A. A. Belik, S. Y. Stefanovich, B. I. Lazoryak, and E. Takayama-Muromachi, Chemistry of Materials **18**, 1964 (2006).

[23] R. Yu, H. Hojo, K. Oka, T. Watanuki, A. Machida, K. Shimizu, K. Nakano, and M. Azuma, Chemistry of Materials **27**, 2012 (2015).

[24] A. A. Belik, Journal of Solid State Chemistry **195**, 32 (2012).

[25] V. Nagarajan *et al.*, Applied Physics Letters **81**, 4215 (2002).

[26] Y. H. Chu, L. W. Martin, Q. Zhan, P. L. Yang, M. P. Cruz, K. Lee, M. Barry, S. Y. Yang, and R. Ramesh, Ferroelectrics **354**, 167 (2007).

[27] D. Kan, L. Palova, V. Anbusathaiah, C. J. Cheng, S. Fujino, V. Nagarajan, K. M. Rabe, and I. Takeuchi, Advanced Functional Materials **20**, 1108 (2010).

[28] H. Hojo, K. Onuma, Y. Ikuhara, and M. Azuma, Applied Physics Express **7**, 091501 (2014).

[29] H. Matsuo *et al.*, Journal of Applied Physics **108**, 104103 (2010).

[30] K. Momma and F. Izumi, Journal of Applied Crystallography **44**, 1272 (2011).

[31] K. Oka, I. Yamada, M. Azuma, S. Takeshita, K. H. Satoh, A. Koda, R. Kadono, M. Takano, and Y. Shimakawa, Inorganic Chemistry **47**, 7355 (2008).

[32] K. Oka *et al.*, Journal of the American Chemical Society **132**, 9438 (2010).

[33] M. Azuma, S. Niitaka, N. Hayashi, K. Oka, M. Takano, H. Funakubo, and Y. Shimakawa, Japanese Journal of Applied Physics **47**, 7579 (2008).

[34] K. Oka, T. Koyama, T. Ozaaki, S. Mori, Y. Shimakawa, and M. Azuma, Angewandte Chemie-International Edition **51**, 7977 (2012).

[35] S. Yasui *et al.*, Japanese Journal of Applied Physics **47**, 7582 (2008).

[36] Y. Nakamura, M. Kawai, M. Azuma, and Y. Shimakawa, Japanese Journal of Applied Physics **49**, 051501 (2010).

[37] Y. Nakamura, M. Kawai, M. Azuma, M. Kubota, M. Shimada, T. Aiba, and Y. Shimakawa, Japanese Journal of Applied Physics **50**, 031505 (2011).

[38] H. Yusa, A. A. Belik, E. Takayama-Muromachi, N. Hirao, and Y. Ohishi, Physical Review B **80**, 214103 (2009).

[39] A. A. Belik, D. A. Rusakov, T. Furubayashi, and E. Takayama-Muromachi, Chemistry of Materials **24**, 3056 (2012).

[40] H. Bea *et al.*, Physical Review Letters **102**, 217603 (2009).

[41] R. J. Zeches *et al.*, Science **326**, 977 (2009).

[42] W. Eerenstein, N. D. Mathur, and J. F. Scott, Nature **442**, 759 (2006).

[43] M. Bibes and A. Barthelemy, Nature Materials **7**, 425 (2008).

[44] T. Kimura, T. Goto, H. Shintani, K. Ishizaka, T. Arima, and Y. Tokura, Nature **426**, 55 (2003).

[45] A. P. Ramirez, Journal of Physics-Condensed Matter **9**, 8171 (1997).

[46] T. Kimura, S. Ishihara, H. Shintani, T. Arima, K. T. Takahashi, K. Ishizaka, and Y. Tokura, Physical Review B **68**, 060403 (2003).

[47] T. Kimura, G. Lawes, T. Goto, Y. Tokura, and A. P. Ramirez, Physical Review B **71**, 224425 (2005).

[48] H. Katsura, N. Nagaosa, and A. V. Balatsky, Physical Review Letters **95**, 4, 057205 (2005).

[49] M. Kenzelmann *et al.*, Physical Review Letters **95**, 087206 (2005).

[50] N. Abe, K. Taniguchi, S. Ohtani, T. Takenobu, Y. Iwasa, and T. Arima, Physical Review Letters **99**, 227206 (2007).

[51] Y. Tokunaga, Y. Taguchi, T. Arima, and Y. Tokura, Nature Physics **8**, 838 (2012).

[52] I. Sosnowska, T. Peterlinneumaier, and E. Steichele, Journal of Physics C-Solid State Physics **15**, 4835 (1982).

[53] M. Tokunaga, M. Azuma, and Y. Shimakawa, Journal of the Physical Society of Japan **79**, 064713 (2010).

[54] H. Yamamoto, T. Kihara, K. Oka, M. Tokunaga, K. Mibu, and M. Azuma, Journal of the Physical Society of Japan **85**, 064704 (2016).

[55] D. Sando *et al.*, Nature Materials **12**, 641 (2013).

[56] C. Ederer and N. A. Spaldin, Physical Review B **71**, 060401(R) (2005).

[57] L. L. Fan, J. Chen, Y. Ren, Z. Pan, L. X. Zhang, and X. R. Xing, Physical Review Letters **116**, 027601 (2016).

[58] D. Damjanovic, Applied Physics Letters **97**, 062906 (2010).

[59] K. A. Schonau, L. A. Schmitt, M. Knapp, H. Fuess, R. A. Eichel, H. Kungl, and M. J. Hoffmann, Physical Review B **75**, 184117 (2007).

[60] Y. M. Jin, Y. U. Wang, A. G. Khachaturyan, J. F. Li, and D. Viehland, Physical Review Letters **91**, 197601 (2003).

[61] T. Asada and Y. Koyama, Physical Review B **75**, 214111 (2007).

[62] H. M. Christen, J. H. Nam, H. S. Kim, A. J. Hatt, and N. A. Spaldin, Physical Review B **83**, 144107 (2011).

[63] Z. H. Chen *et al.*, Applied Physics Letters **97**, 242903 (2010).

[64] Z. H. Chen *et al.*, Advanced Functional Materials **21**, 133 (2011).

[65] Z. Fan *et al.*, Acs Applied Materials & Interfaces **7**, 2648 (2015).

[66] S. Fujino, M. Murakami, V. Anbusathaiah, S. H. Lim, V. Nagarajan, C. J. Fennie, M. Wuttig, L. Salamanca-Riba, and I. Takeuchi, Applied Physics Letters **92**, 202904 (2008).

[67] C. J. Cheng, D. Kan, S. H. Lim, W. R. McKenzie, P. R. Munroe, L. G. Salamanca-Riba, R. L. Withers, I. Takeuchi, and V. Nagarajan, Physical Review B **80**, 014109 (2009).

[68] K. T. Ko *et al.*, Nature Communications **2**, 567 (2011).

[69] C. Beekman *et al.*, Advanced Materials **25**, 5561 (2013).

[70] A. R. Damodaran, C. W. Liang, Q. He, C. Y. Peng, L. Chang, Y. H. Chu, and L. W. Martin, Advanced Materials **23**, 3170 (2011).

[71] J. X. Zhang *et al.*, Nature Nanotechnology **6**, 97 (2011).

[72] J. Rouquette, J. Haines, V. Bornand, M. Pintard, P. Papet, W. G. Marshall, and S. Hull, Physical Review B **71**, 10, 024112 (2005).

[73] R. Z. Yu, N. Matsuda, K. Tominaga, K. Shimizu, H. Hojo, Y. Sakai, H. Yamamoto, K. Oka, and M. Azuma, Inorganic Chemistry **55**, 6124 (2016).

[74] L. Chen, V. Nagarajan, R. Ramesh, and A. L. Roytburd, Journal of Applied Physics **94**, 5147 (2003).

[75] M. Budimir, D. Damjanovic, and N. Setter, Physical Review B **72**, 064107 (2005).

[76] M. Budimir, D. Damjanovic, and N. Setter, Physical Review B **73**, 174106 (2006).

[77] P. Baettig, C. F. Schelle, R. LeSar, U. V. Waghmare, and N. A. Spaldin, Chemistry of Materials **17**, 1376 (2005).

[78] H. J. Liu, P. Yang, Z. Fan, A. Kumar, K. Yao, K. P. Ong, K. Y. Zeng, and J. Wang, Physical Review B **87**, 220101 (2013).

[79] X. H. Du, U. Belegundu, and K. Uchino, Japanese Journal of Applied Physics Part 1-Regular Papers Short Notes & Review Papers **36**, 5580 (1997).

[80] M. Budimir, D. Damjanovic, and N. Setter, Journal of Applied Physics **94**, 6753 (2003).

[81] D. Damjanovic, Journal of the American Ceramic Society **88**, 2663 (2005).

[82] F. Matsukura, Y. Tokura, and H. Ohno, Nature Nanotechnology **10**, 209 (2015).

[83] Y. Tokunaga, N. Furukawa, H. Sakai, Y. Taguchi, T. H. Arima, and Y. Tokura, Nature Materials **8**, 558 (2009).

[84] J. M. Moreau, C. Michel, R. Gerson, and W. J. James, Journal of Physics and Chemistry of Solids **32**, 1315 (1971).

[85] A. M. Glazer, Acta Crystallographica Section B-Structural Science **B28**, 3384 (1972).

[86] P. Fischer, M. Polomska, I. Sosnowska, and M. Szymanski, Journal of Physics C-Solid State Physics **13**, 1931 (1980).

[87] D. L. Vinokurov and A. I. Morozov, Physics of the Solid State **57**, 1781 (2015).

[88] H. Hojo, R. Kawabe, K. Shimizu, H. Yamamoto, K. Mibu, K. Samanta, T. Saha-Dasgupta, and M. Azuma, Advanced Materials **29**, 1603131 (2017).

[89] A. Agbelele *et al.*, Advanced Materials **29**, 1602327 (2017).

[90] D. Kan and I. Takeuchi, Journal of Applied Physics **108,** 014104 (2010).

[91] K. Shimizu, H. Hojo, Y. Ikuhara, and M. Azuma, Advanced Materials **28**, 8639 (2016).

[92] H. Dixit, J. H. Lee, J. T. Krogel, S. Okamoto, and V. R. Cooper, Scientific Reports **5**, 12969 (2015)..

[93] Y. H. Chu *et al.*, Advanced Materials **18**, 2307 (2006).

[94] H. W. Jang *et al.*, Advanced Materials **21**, 817 (2009).

[95] N. Balke, S. Choudhury, S. Jesse, M. Huijben, Y. H. Chu, A. P. Baddorf, L. Q. Chen, R. Ramesh, and S. V. Kalinin, Nature Nanotechnology **4**, 868 (2009).

[96] S. Matzen, O. Nesterov, G. Rispens, J. A. Heuver, M. Biegalski, H. M. Christen, and B. Noheda, Nature Communications **5**, 8, 4415 (2014).

[97] A. Crassous, T. Sluka, A. K. Tagantsev, and N. Setter, Nature Nanotechnology **10**, 614 (2015).

[98] C. Liu, J. Ma, Y. J. Zhang, J. H. Chen, and C. W. Nan, AIP Advances **7**, 6, 055003 (2017).

[99] S. H. Baek *et al.*, Nature Materials **9**, 309 (2010).

[100] Y. H. Chu *et al.*, Applied Physics Letters **92**, 3, 102909 (2008).

Acknowledgements

First, I would like to thank my supervisor Prof. Masaki Azuma for his enthusiastic guidance.

I would like to acknowledge Prof. Hiroshi Funakubo, Prof. Mamoru Yoshimoto, Prof. Takao Sasagawa, and Prof. Tomoyasu Taniyama for useful suggestions and comments.

I am deeply grateful to former assistant Prof. Hajime Hojo (Assoc. Prof. in Kyushu University, currently) and former assistant Prof. Kengo Oka (assistant Prof. in Chuo University, currently) and current assistant professor Kei Shigematsu.

I would like to express my gratitude to Prof. Yu Kumagai (Tokyo Tech.), Prof. Fumiyasu Oba (Tokyo Tech.), Mr Motoya Suzuki (Tokyo Tech.), Prof. Ko Mibu (Nagoya Institute of Technology), and Prof. Yuichi Ikuhara (University of Tokyo) for their collaboration and fruitful discussion.

I would like to thank members in the Azuma group; Ms. Rie Hashiguchi and Ms. Chika Sakaguchi, Dr. Yuki Sakai (KISTEC), Dr. Runze Yu (IOP CAS, currently), Dr. Kosuke Nishimura (Shoei chemical Inc.), Dr. Makoto Kubota (Canon Inc.), Mr. Ko Onuma, Mr. Yuya Muramatsu, Mr. Koichiro Nabetani, Dr. Zhao Pan, Mr. Hajime Yamamoto, Ms. Kiho Nakano Nabetani, Mr. Kantaro Arai, Mr. Ryo Kawabe, Ms. Narumi Matsuda, Mr. Ken Tominaga, Mr. Takahiro Ogata, Mr. Takeshi Asakura, Mr. Yuichiro Hattori, Mr. Takumi Nishikubo, Ms. Saki Fujiwara, Mr. Hirokazu Kyokane, Mr. Haruki Shimizu, Mr Tatsuru Yamamoto, Mr. Takashi Imai, Mr. Koki Maebayashi, Mr. Kazumasa Yamamoto, Mr. Hayato Ishizaki, and Ms. Marin Katsumata.

Finally I deeply appreciate my family for their support.

Accomplishments

List of publications

[1] Keisuke Shimizu, Hajime Hojo, Yuichi Ikuhara, Masaki Azuma, "Enhanced Piezoelectric Response due to Polarization Rotation in Cobalt-Substituted $BiFeO_3$ Epitaxial Thin Films", Adv. Mater. **28**, 8639 (2016).

[2] Keisuke Shimizu, Ryo Kawabe, Hajime Hojo, Haruki Shimizu, Hajime Yamamoto, Kei Shigematsu, Ko Mibu, Yu Kumagai, Fumiyasu Oba and Masaki Azuma, "Direct observation of magnetization reversal by electric field at room temperature in Co substituted bismuth ferrite thin film" *submitted*.

[3] Keisuke Shimizu, Hajime Hojo, and Masaki Azuma, "Orientation dependence of piezoelectric properties of $BiFe_{1-x}Ga_xO_3$ thin films with a giant *c*/*a* ratio" *in preparation*.

Other publications

[4] Keisuke Shimizu, Kei Shigematsu, and Masaki Azuma, "Fabrication of high-pressure stable quadruple perovskite $LnCu_3Mn_4O_{12}$ epitaxial thin films with room-temperature ferrimagnetism" *in preparation*.

[5] Runze Yu, Hajime Hojo, Kengo Oka, Tetsu Watanuki, Akihiko Machida, Keisuke Shimizu, Kiho Nakano, and Masaki Azuma, "New $PbTiO_3$-Type Giant Tetragonal Compound Bi_2ZnVO_6 and Its Stability under Pressure", Chem. Mater. **27**, 2012 (2015).

[6] Runze Yu, Narumi Matsuda, Ken Tominaga, Keisuke Shimizu, Hajime Hojo, Yuki Sakai, Hajime Yamamoto, Kengo Oka, Masaki Azuma, "High-Temperature Monoclinic *Cc* Phase with Reduced *c*/*a* Ratio in Bi-based Perovskite Compound $Bi_2ZnTi_{1-x}Mn_xO_6$", Inorg. Chem. **55**, 6124 (2016).

[7] Hajime Hojo, Ryo Kawabe, Keisuke Shimizu, Hajime Yamamoto, Ko Mibu, Kartik Samanta, Tanusri Saha - Dasgupta, Masaki Azuma, "Ferromagnetism at Room Temperature Induced by Spin Structure Change in $BiFe_{1-x}Co_xO_3$ Thin Films", Adv. Mater. 29, 1603131 (2017).

List of presentations

International conferences

[1] Keisuke Shimizu, Ko Onuma, Hajime Hojo, and Masaki Azuma, "Crystal and domain structure of the Co-substituted $BiFeO_3$ thin films on $LaAlO_3$ substrates", The Eighth International Conference on the Science and Technology for Advanced Ceramics (STAC8), Mielparque-Yokohama, Yokohama, Japan, June, 2014

[2] Keisuke Shimizu, Hajime Hojo, and Masaki Azuma, "Crystal structures and piezoelectric properties in $BiFe_{1-x}Co_xO_3$ thin films with a giant *c*/*a* ratio", 17th US-Japan Seminar on Dielectric and Piezoelectric Ceramics, Hotel Buena Vista, Matsumoto, Japan, November, 2015

[3] Keisuke Shimizu, Hajime Hojo, Yuichi Ikuhara, and Masaki Azuma, "Enhanced piezoelectric response due to polarization rotation in cobalt-substituted $BiFeO_3$ epitaxial thin films" 2016 MRS fall meeting, Boston, USA, Nov.-Dec., 2016

[4] Keisuke Shimizu, Hajime Hojo, Yuichi Ikuhara, and Masaki Azuma, "Enhanced piezoelectric response due to polarization rotation in Co-substituted $BiFeO_3$ epitaxial thin films", 2017 Joint IEEE ISAF-IWATMD-PFM, Georgia Institute of Technology, Atlanta, USA, May, 2017

[5] Keisuke Shimizu, Hajime Hojo, Yuichi Ikuhara, and Masaki Azuma, "Enhanced piezoelectric response due to polarization rotation in cobalt-substituted $BiFeO_3$ epitaxial thin films", JSPM International Conference on Powder and Powder Metallurgy ~ 60th Anniversary~, Kyoto University, Kyoto, Japan, November, 2017

[6] Keisuke Shimizu, Ryo Kawabe, Hajime Yamamoto, Hajime Hojo, Kei Shigematsu, and Masaki Azuma, "Direct observation of magnetization reversal by polarization switching in multiferroic Co-substituted $BiFeO_3$ thin film", The 9^{th} APCTP Workshop on Multiferroics, University of Tokyo, Kashiwa, Japan, November, 2017

[7] Keisuke Shimizu, Hajime Hojo, and Masaki Azuma, "Polarization rotation in $BiFe_{1-x}Co_xO_3$ and $BiFe_{1-x}Ga_xO_3$ epitaxial thin films", ISNTE-II, Tokyo Institute of Technology, Yokohama, Japan, December, 2017

Domestic conferences

[1] Keisuke Shimizu, Ko Onuma, Hajime Hojo, and Masaki Azuma, "$BiFe_{0.9}Co_{0.1}O_3$ エピタキシャル薄膜の電気特性の酸素分圧依存性"、Autumn Meeting of the Japan Society of Powder and Powder Metallurgy 2013, Nagoya Congress Center, Nagoya, November, 2013

[2] Keisuke Shimizu, Ko Onuma, Hajime Hojo, and Masaki Azuma, "Effect of Oxygen Pressure on Electrical properties of $BiFe_{0.90}Co_{0.1}O_3$ epitaxial thin films"、The 52nd Symposium on Basic Science of Ceramics, Winc-aichi, Nagoya, January, 2014

[3] Keisuke Shimizu, Hajime Hojo, and Masaki Azuma, "Fabrication of $BiFe_{1-x}Co_xO_3$ thin films with a giant *c*/*a* ratio, crystal structures, and electronic properties", The 75th JSAP Autumn Meeting, Hokkaido University, Sapporo, September, 2014

[4] Keisuke Shimizu, Hajime Hojo, and Masaki Azuma, "巨大な *c*/*a* 比を有する $BiFe_{1-x}Co_xO_3$ 薄膜の作製とその結晶構造および電気的特性", The 4th CSJ Chemistry Festa, Tower Hall Funabori, Tokyo, October, 2014

[5] Keisuke Shimizu, Hajime Hojo, and Masaki Azuma, "Crystal structures and piezoelectric properties in $BiFe_{1-x}Co_xO_3$ thin films with a giant *c*/*a* ratio"、 The 62th JSAP Spring Meeting, Tokai University, Hiratsuka, March, 2015

[6] Keisuke Shimizu, Hajime Hojo, and Masaki Azuma, "Fabrication of $BiFe_{1-x}Co_xO_3$ thin films with a giant *c*/*a* ratio and their crystal structures and electronic properties", The 32th Meeting on Ferroelectric Materials and Their Applications (FMA32), CO-OP INN Kyoto, Kyoto, May, 2015

[7] Keisuke Shimizu, Hajime Hojo, and Masaki Azuma, "Preparation and orientation control of Ga-substituted bismuth ferrite thin films with a giant *c*/*a* ratio", The 63th JSAP Spring Meeting, Tokyo Institute of Technology, Tokyo, March, 2016

[8] Keisuke Shimizu, Ryo Kawabe, Hajime Hojo, Hajime Yamamoto, Ko Mibu, and Masaki Azuma, "Observation of magnetization switching by electric field in $BiFe_{0.9}Co_{0.1}O_3$ thin films", The 64th JSAP Spring Meeting, Pacifico Yokohama, Yokohama, March, 2017

[9] Keisuke Shimizu, Kei Shigematsu, and Masaki Azuma, “Fabrication of room-temperature ferrimagnetic quadruple perovskite $LnCu_3Mn_4O_{12}$ thin films”, The 78th JSAP Autumn Meeting, Fukuoka Convention Center, Fukuoka, September, 2017